1 **TITLE**

2 Lysine63-linked ubiquitin chains earmark GPCRs for BBSome-
3 mediated removal from cilia

4 **AUTHORS:** Swapnil Rohidas Shinde, Andrew R. Nager[#] and Maxence V. Nachury[*]

5 **AFFILIATION:**

6 Department of Ophthalmology, University of California San Francisco, CA 94143, USA

7

8 * Correspondence: maxence.nachury@ucsf.edu

9 # Current address: Cancer Immunology Discovery, Pfizer Inc., San Diego, CA, 92121, USA

ABSTRACT (160 words)

G-protein coupled receptors (GPCRs) undergo regulated trafficking into and out of cilia to control cilium-based signaling pathways. β-arrestin 2, a molecular sensor of activated GPCRs, and the BBSome are required for the signal-dependent exit of ciliary GPCRs but it is not known how β-arrestin 2 relays the activation state of GPCRs to the ciliary exit machinery. Here we find that, upon activation, the ciliary GPCRs SSTR3 and GPR161 become tagged with K63-linked ubiquitin (K63Ub) chains in a β-arrestin 2-dependent manner prior to BBSome-mediated exit. Removal of ubiquitin acceptor residues from SSTR3 and GPR161 demonstrates that ubiquitination of ciliary GPCRs is required for their regulated exit from cilia. Furthermore, targeting a K63Ub-specific deubiquitinase to cilia blocks the exit of GPR161, SSTR3 and SMO from cilia. Finally, ubiquitinated proteins accumulate in cilia of mammalian photoreceptors and *Chlamydomonas* cells. We conclude that K63Ub chains mark GPCRs and other unwanted ciliary proteins for recognition by the ciliary exit machinery.

INTRODUCTION

The regulated trafficking of signaling receptors in and out of cilia is a near-universal feature of cilia-based signaling pathways that is germane to the transduction of signals (Nachury and Mick, 2019; Anvarian et al., 2019; Mykytyn and Askwith, 2017). For example, in Hedgehog signaling, pathway activation leads to the disappearance of the Hedgehog receptor Patched 1 and of the G protein-coupled receptor (GPCR) GPR161 from cilia and to the concurrent accumulation of the GPCR Smoothened (SMO) in cilia (Rohatgi et al., 2007; Corbit et al., 2005; Mukhopadhyay et al., 2013). In all three cases, regulated exit from cilia plays a major role in the on-demand redistribution of signaling molecules (Nachury and Mick, 2019). Signal-dependent exit has been generalized to every ciliary GPCRs studied to date. The Somatostatin Receptor 3 (SSTR3), Dopamine Receptor 1 (D1R), Melanocortin concentrating hormone receptor 1 (MCHR1), the neuropeptide receptor 2 (NPY2R) all disappear from cilia upon exposure to agonist (Domire et al., 2011; Loktev and Jackson, 2013; Nager et al., 2017; Green et al., 2015). A major question is how GPCRs are selected for removal from cilia only under specific conditions (typically upon activation).

Two major trafficking modules participate directly in signal-dependent exit from cilia. First, the BBSome is an evolutionarily conserved complex of eight Bardet-Biedl Syndrome (BBS) proteins that directly recognizes intracellular determinants in GPCRs and ferries them out of cilia (Nachury, 2018; Wingfield et al., 2018). The BBSome associates with the intraflagellar transport (IFT) machinery and has been proposed to act as adaptor between the motor-driven intraflagellar transport trains and the membrane proteins that are to be removed from cilia. Second, β-arrestin 2 is a well-established molecular sensor of the activation state of GPCRs that is required for the signal-dependent exit of GPR161 and SSTR3 (Pal et al., 2016; Green et al., 2015; Nager et al., 2017). No association of β-arrestin 2 with ciliary trafficking complexes has been reported to date and it remains unclear how β-arrestin 2 relays information regarding the state of activation of ciliary GPCRs to the ciliary exit machinery.

An emerging player in ciliary exit is ubiquitination (Shearer and Saunders, 2016). Ubiquitin (Ub), a 76-amino acid polypeptide, becomes conjugated to acceptor lysine residues on substrate

53 proteins by ubiquitin ligases and routes substrates for degradation or other regulatory fates (Yau
54 and Rape, 2016; Swatek and Komander, 2016). A role for ubiquitin in promoting ciliary exit is
55 suggested by multiple lines of evidence. First, interfering with Patched1 ubiquitination blocks its
56 signal-dependent exit from cilia (Kim et al., 2015; Yue et al., 2014). Second, fusing ubiquitin to
57 the cytoplasmic tails of PKD-2, of the olfactory receptor ODR-10 or of the TRP channel OSM-9
58 results in the disappearance of these proteins from cilia (Hu et al., 2007; Xu et al., 2015). The
59 accumulation of these ubiquitin-protein fusions inside cilia when BBSome function is
60 compromised suggests that the BBSome might sort ubiquitinated signaling receptors out of cilia,
61 in line with a reported association of BBSome with ubiquitinated proteins in trypanosomes
62 (Langousis et al., 2016). Interestingly, TRIM32 is a ubiquitin ligase that is mutated in BBS
63 patients in one consanguineous family and interference with TRIM32 function in zebrafish
64 produces typical BBS-related phenotypes (Chiang et al., 2006). Third, the ubiquitin ligase Cbl is
65 recruited to cilia upon activation of the ciliary tyrosine kinase receptor PDGFRαα and Cbl is
66 required for termination of PDGFRαα signaling (Schmid et al., 2018). Last, a dramatic rise in
67 ubiquitination of the ciliary proteome is observed when *Chlamydomonas* cilia disassemble (Huang
68 et al., 2009). In particular, α-tubulin becomes ubiquitinated on K304 upon cilia disassembly and
69 expression of α-tubulin[K304R] slows down cilia disassembly (Wang et al., 2019).
70 Together, these data led us to investigate the interplay between ubiquitination, β-arrestin 2 and
71 the ciliary exit machinery. Given the well-established function of β-arrestin 2 in directing
72 activation-dependent ubiquitination of GPCRs on the surface of endosomes (Henry et al., 2012;
73 Bhandari et al., 2007; Shenoy et al., 2008), we posited that β-arrestin 2 may direct the activation-
74 dependent ubiquitination of ciliary GPCRs and that ubiquitinated GPCRs are selected by the
75 BBSome for removal from cilia.

76 **RESULTS**

77 **Signal-dependent ubiquitination of ciliary GPCRs is required for their regulated**
78 **exit from cilia**

79 A central prediction of the above model is that the activation of ciliary GPCRs will lead to their
80 ubiquitination inside cilia prior to BBSome-mediated retrieval. We blocked BBSome-dependent
81 exit by deleting its cognate GPTase ARL6/BBS3 and monitored ciliary ubiquitin levels by
82 immunostaining. When SSTR3 was expressed in *Arl6*$^{-/-}$ IMCD3 cells, addition of its agonist
83 somatostatin (sst) led to a drastic increase in the ciliary levels of ubiquitin as reported by the well-
84 characterized FK2 (**Figure 1A-B)** and FK1 (**Figure S1A-B**) monoclonal antibodies (Fujimuro
85 et al., 1994; Emmerich and Cohen, 2015; Haglund et al., 2003). As the two antibodies have
86 identical selectivity for ubiquitin species, all further experiments were conducted with the FK2
87 antibody. Because the sst-dependent increase in ciliary ubiquitin signal was no longer observed in
88 the absence of SSTR3 expression (**Figure 1A-B and S1C-D**), these results indicate that SSTR3
89 itself becomes ubiquitinated inside cilia upon activation. We noted that ciliary ubiquitin was
90 already detectable in the absence of sst in *Arl6*$^{-/-}$ cells. This ciliary ubiquitin signal did not depend
91 upon expression of SSTR3 (compare 3rd and 5th violin plots in **Figure 1B**) and suggests that a
92 GPCR endogenous to IMCD3 cells may become activated and ubiquitinated inside *Arl6*$^{-/-}$ cilia
93 under our culture conditions. No ubiquitin signal was detected in cilia when BBSome function
94 was intact (**Figure 1A-B and S1A-D**), indicating that the BBSome efficiently removes
95 ubiquitinated GPCRs from cilia.

96 One signaling pathway that is natively expressed in IMCD3 cells is the Hedghog pathway. Prior
97 experiments have detected normal trafficking dynamics of SMO and GPR161 in IMCD3 cells
98 (Ye et al., 2018; Mukhopadhyay et al., 2013) and **Figure 4B**). GPR161 and SMO both
99 accumulate in cilia of *Arl6*$^{-/-}$ cells (Liew et al., 2014; Zhang et al., 2011) and it is conceivable that
100 the ubiquitin signal detected in cilia corresponds to ubiquitin conjugated to SMO or GPR161.
101 Activation of SMO by small molecule agonists normally triggers exit of GPR161 but this exit is
102 frustrated when BBSome function goes awry. We detected a significant elevation of the ciliary

103 ubiquitin levels in *Arl6*$^{-/-}$ cells when treated with the SMO agonist SAG (**Figure 1C-D**),
104 suggesting that GPR161 may get ubiquitinated prior to its BBSome-dependent exit. Collectively,
105 these data suggest that GPCRs are ubiquitinated in a regulated fashion inside cilia and
106 subsequently retrieved into the cell by the BBSome.

107 To test the functional importance of GPCR ubiquitination in BBSome-mediated exit from cilia,
108 we removed all ubiquitination sites from SSTR3 and GPR161 by mutating all cytoplasm-
109 exposed lysine residues to arginine (cK0 variants). In both cases, the cK0 variant underwent
110 markedly slower signal-dependent exit from cilia than the WT allele (**Figure 1E-F**).
111 Measurement of exit rates revealed that exit of SSTR3cK0 was ~2-fold slower than SSTR3 and
112 that exit of GPR161cK0 was ~2.5-fold slower than GPR161. These results strongly support a
113 role for GPCR ubiquitination in promoting signal-dependent exit from cilia

114

115 **K63-linked ubiquitin chains inside cilia are required for GPCR exit**

116 We next sought to characterize the type of ubiquitin conjugates that are attached to ciliary
117 proteins. A single ubiquitin can be conjugated to substrates (monoubiquitination) or lysine
118 residues on ubiquitin can be conjugated to another ubiquitin molecule for building ubiquitin
119 chains (polyubiquitination). Lys48 and Lys 63 are the most prevalent ubiquitin chain linkages
120 with K48 serving as a targeting signal for proteasomal degradation of soluble proteins and K63
121 serving as a lysosomal sorting signal for membrane proteins or a signal for regulated interactions
122 (Yau and Rape, 2016; Swatek and Komander, 2016). The FK1 and FK2 antibodies used above
123 recognizes ubiquitin either as single adduct or in chain but does not recognize free ubiquitin
124 (Fujimuro et al., 1994; Emmerich and Cohen, 2015). The availability of antibodies specific for
125 K48 and K63 ubiquitin linkages (Newton et al., 2008) enabled us to determine the types of
126 ubiquitin conjugates that are attached to ciliary GPCRs. While we found no detectable signal for
127 K48-linked ubiquitin chains (UbK48) in cilia, the for K63-linked ubiquitin (UbK63) chains
128 mirrored the ciliary response observed with the FK2 antibody in IMCD3-[SSTR3] cells

129 subjected to agonist treatment (**Figure 2 and S1E-F**). We conclude that K63Ub chains are
130 added onto SSTR3 inside cilia upon activation.

131 To determine the functional importance of UbK63 linkages in tagging GPCRs for exit from cilia,
132 we devised a strategy that cleaves UbK63 linkages inside cilia (**Figure 3A**). Structural and
133 biochemical studies have demonstrated that the deubiquitinase AMSH possesses a near-absolute
134 specificity for UbK63 linkages and does not cleave other Ub chain linkages or Ub-substrates
135 linkages (Sato et al., 2008; McCullough et al., 2004). We targeted AMSH to cilia using the well-
136 validated ciliary targeting signal from the ciliopathy protein NPHP3 (Nakata et al., 2012; Wright
137 et al., 2011, 3) and analyzed the exit of three distinct GPCRs: SMO, GPR161 and SSTR3. To
138 alleviate concerns related to the interaction of AMSH with the ESCRT-0 protein STAM
139 (McCullough et al., 2006), we deleted the STAM-interacting domain of AMSH and only
140 expressed the catalytic domain of AMSH. The signal-dependent exit of SSTR3 was assessed by
141 treating IMCD3-[SSTR3] cells with sst for 2h. In cells expressing cilia-AMSH (a fusion of
142 NPHP3[1-200] to GFP and the catalytic domain of AMSH), sst failed to bring a significant
143 reduction in the ciliary levels of SSTR3 (**Figure 3B-C**). Care was taken to only analyze cells that
144 expressed modest levels of cilia-AMSH as judged by GFP fluorescence. In contrast, SSTR3 exit
145 proceeded normally in cells that expressed NPHP3[1-200]-GFP alone or a catalytically dead
146 variant of cilia-AMSH that we named cilia-ASMH† (**Figure 3B-C**). These controls demonstrate
147 that cilia-AMSH exerts its effects on SSTR3 exit by cleaving UbK63 chains inside cilia.
148 Similarly, the exit of endogenous GPR161 from RPE cell cilia upon activation of the Hedgehog
149 pathway was abolished in cells expressing moderate levels of cilia-AMSH (**Figure 3D-E**).
150 Neither NPHP3[1-200]-GFP nor cilia-AMSH† blocked the signal-dependent exit of GPR161
151 from cilia (**Figure 3D-E**).

152 Unlike GPR161 and other ciliary GPCRs such as the Somatostatin receptor 3 (SSTR3) that are
153 removed from cilia by the BBSome only when they become activated, SMO undergoes
154 constitutive BBSome-dependent exit from cilia in the absence of Hedgehog pathway stimulation.
155 Signal-dependent accumulation of SMO in cilia is achieved, at least in part, by suppression of its
156 exit (Milenkovic et al., 2015; Nachury and Mick, 2019; Ye et al., 2018). In cells expressing cilia-

157 AMSH, endogenous SMO spontaneously accumulated inside cilia in the absence of Hedgehog
158 pathway activation (**Figure 3F-G**). Again, neither NPHP3[1-200]-GFP nor cilia-AMSH†
159 influenced the ciliary accumulation of SMO (**Figure 3F-G**).

160 Together, these results indicate that K63-linked ubiquitin chains inside cilia, presumably built
161 onto each ciliary GPCRs under a specific signaling stimulus, are required for GPCR removal
162 from cilia.

163

164 **β-arrestin 2 mediates signal-dependent ubiquitination of ciliary GPCRs**

165 As β-arrestin 2 is required for signal-dependent exit of GPR161 and SSTR3 from cilia (Green et
166 al., 2015; Pal et al., 2016; Ye et al., 2018), we sought to determine the functional relationship
167 between β-arrestin 2 and the BBSome. As previously described (Green et al., 2015), β-arrestin 2
168 is initially undetectable inside cilia and becomes recruited to cilia within minutes of SSTR3
169 agonist addition (**Figure 4A-C**). The ciliary β-arrestin 2 signal reaches its maximum in 10 min
170 and the $t_{1/2}$ for ciliary accumulation is less than 5 min (**Figure 4C**). Meanwhile the $t_{1/2}$ for
171 BBSome recruitment to the tip of cilia was 10 min and the first signs of detectable SSTR3 exit
172 were seen between 10 and 15 min (**Figure 4C**). These kinetics suggested the following sequence
173 of events: β-arrestin 2 first becomes recruited to activated ciliary SSTR3, then the BBSome
174 ferries activated SSTR3 out of cilia. When ARL6 was depleted, the basal levels of ciliary β-
175 arrestin 2 were elevated but the kinetics of β-arrestin 2 accumulation in cilia upon SSTR3
176 activation were indistinguishable from control-depleted cells (**Figure 4A-B**). These data suggest
177 that a fraction of SSTR3 that accumulates in cilia of ARL6-depleted cells is tonically active and
178 recruit β-arrestin 2. From these data, we conclude that β-arrestin 2 functions either upstream of,
179 or in parallel with the BBSome in signal-dependent retrieval of GPCRs. Similarly, the kinetics of
180 GPR161 exit and β-arrestin 2 ciliary recruitment upon activation of the Hh pathway indicated
181 that β-arrestin 2 reaches its maximal ciliary level before the first signs of GPR161 exit become
182 evident (**Figure 4D**).

183 We previously proposed that β-arrestin 2 may directly stabilize the interaction of the BBSome
184 with its GPCR cargoes (Ye et al., 2018). Yet, we have thus far failed to detect a biochemical
185 interaction between β-arrestin 2 and the BBSome. Furthermore, a direct binding to the GPCR-
186 BBSome complexes predicts that β-arrestin 2 co-localizes with IFT trains inside cilia. Against this
187 hypothesis, β-arrestin 2 was evenly distributed inside cilia (**Figure 4A**), reminiscent of the
188 distribution pattern of SSTR3 and distinct from the discontinuous pattern of the BBSome inside
189 cilia.

190 These data lead us to pursue the hypothesis that β-arrestin 2 licenses activated GPCRs for
191 recognition by the BBSome by promoting activation-dependent ubiquitination of GPCRs. The
192 rationale for this hypothesis is two-fold. First, β-arrestin has been shown to function in the signal-
193 dependent targeting of GPCRs from the plasma membrane to the lysosome by directing the
194 recruitment of ubiquitin ligases to activated GPCRs (Henry et al., 2012; Bhandari et al., 2007;
195 Shenoy et al., 2008). Ubiquitinated GPCRs are sorted to the degradative route via ESCRT
196 complexes and associated ubiquitin recognition modules. Second, ubiquitination promotes ciliary
197 exit of the signaling receptor and BBSome cargoes Patched 1 (Kim et al., 2015; Yue et al., 2014),
198 GPR161, SSTR3 and SMO (**Figures 1E-F and 3B-G**).

199 We thus considered the model that β-arrestin 2 recruits ubiquitin ligases to activated GPCR and
200 ubiquitinated GPCRs are then selected by the BBSome for removal from cilia. A central
201 prediction of this model is that the activation of ciliary GPCRs will lead to their β-arrestin 2-
202 dependent ubiquitination inside cilia prior to BBSome-mediated retrieval. To test this prediction,
203 we leveraged IMCD3 cell lines deleted for *Arl6* alone or for both *Arl6* and *β-arrestin 2* (Nager et
204 al., 2017). When IMCD3 *Arl6*$^{-/-}$ cells stably expressing SSTR3 were treated with sst, SSTR3 exit
205 from cilia failed and ubiquitin staining in cilia concomitantly rose (**Figures 1A-B and 4E-F**),
206 indicating that SSTR3 undergoes signal-dependent ubiquitination. In cells deleted for both *Arl6*
207 and *β-arrestin 2*, SSTR3 exit still failed but the rise in ciliary ubiquitin signal upon sst addition was
208 no longer observed (**Figures 4E-F**). Similarly, the increase in ciliary ubiquitin signal seen in *Arl6*$^{-}$
209 $^{/-}$ cells treated with the Hedgehog pathway agonist SAG was no longer observed in the absence of
210 *β-arrestin 2* (**Figure 4G-H**). These data indicate that, in the absence of BBSome function, ciliary

211 GPCRs become ubiquitinated in response to activation in a *β-arrestin 2*-dependent manner.
212 Taken together with the requirements for β-arrestin 2 and for ubiquitination in SSTR3 and
213 GPR161 exit, these data suggest the following order of action: GPCR activation, β-arrestin 2
214 recruitment, assembly of K63Ub chains on the GPCR, and selection of ubiquitinated GPCRs for
215 BBSome-mediated retrieval (**Figure 5E**).

216

217 **Constitutively retrieved BBSome cargoes are ubiquitinated prior to exit**

218 Besides removing GPCRs from cilia in a regulated fashion, the BBSome also clears cilia of
219 unwanted proteins that accidentally enter cilia. Phospholipase D, an AMP kinase family member
220 and a truncated hemoglobin are the major proteins that accumulate in cilia of *Chlamydomonas*
221 Bbs4 mutants (Lechtreck et al., 2009) and it is likely that a range of less abundant proteins may
222 accumulate in *Bbs4* cilia. When stained for ubiquitin, *Bbs4 Chlamydomonas* showed a 2-fold
223 enrichment in ciliary signal compared to WT (**Fig. 5A-B**). Isolation of cilia revealed the
224 accumulation of ubiquitin conjugates above 80 kDa in *Bbs4* mutant *Chlamydomonas* cilia (**Fig.**
225 **5C**). These results are consistent with the hypothesis that ciliary proteins subject to constitutive
226 retrieval are ubiquitinated prior to their removal from cilia by the BBSome.

227 In the mammalian retina, proteomics studies have found over 100 proteins accumulating in the
228 outer segment (the equivalent of the cilium) of *Bbs* photoreceptors compared to WT
229 photoreceptors (Datta et al., 2015). When we stained sections of mouse retina for ubiquitin, we
230 found a drastic accumulation of ubiquitin signal in the outer segment of *Bbs4*$^{-/-}$ photoreceptors
231 compared to WT photoreceptors (**Fig. 5D**). These results suggest that variety of proteins that
232 accidentally flow into the photoreceptors outer segments –possibly caught on the tremendous flux
233 of rhodopsin trafficking to the outer segment (Baker et al., 2008)– are recognized as foreign to the
234 cilium, ubiquitinated on site and selected for removal by the BBSome (**Figure 5E**).

235 **DISCUSSION**

236 **Recognition of K63-linked ubiquitin chains by the ciliary exit machinery**

237 Our results indicate that K63-linked ubiquitin chains tag activated GPCRs and other unwanted
238 proteins for BBSome-mediated removal from cilia. Prior findings in trypanosomes suggest that
239 the BBSome may directly recognize ubiquitin (Langousis et al., 2016), although direct
240 biochemical evidence and information regarding ubiquitin chain specificity is still missing. It is
241 also known that the BBSome directly recognizes cytoplasmic determinants in the GPCRs it
242 ferries out of cilia (Jin et al., 2010; Klink et al., 2017; Ye et al., 2018; Seo et al., 2011; Domire et
243 al., 2011). We propose that the summation of weak molecular interactions between the BBSome
244 and UbK63 chains on one hand and the BBSome and GPCRs cytoplasmic loops on the other
245 hand increases the BBSome-cargo interaction to enable sorting of ubiquitinated GPCRs out of
246 cilia. In support of this bivalent recognition of ubiquitinated cargoes by the BBSome, the affinity
247 of the BBSome for cytoplasmic determinant of GPCRs have been measured to be in the μM
248 range (Klink et al., 2017) and affinities of ubiquitin-binding proteins for ubiquitin typically reside
249 in the sub mM range (Husnjak and Dikic, 2012). The nature of the biochemical entity that
250 directly recognizes ubiquitin, and in particular UbK63 chains remains to be determined: while
251 the BBSome was pulled down on Ub-agarose resin from trypanosome lysate (Langousis et al.,
252 2016), no known Ub-binding domain is found encoded within the BBSome polypeptides.
253 Furthermore, the IFT-A subunit IFT-139 associates with ubiquitinated α-tubulin in ciliary
254 extracts from *Chlamydomonas*, suggesting a possible recognition of ubiquitin by IFT139 (Wang et
255 al., 2019). Again, the absence of known Ub-binding domain in the sequence of IFT139 presents
256 a challenge to this hypothesis.

257 The suppression of GPR161, SSTR3 and SMO exit by cilia-AMSH (**Figure 3**) indicate that
258 UbK63 chains are recognized inside cilia to direct trafficking out of cilia. Similarly, (Wang et al.,
259 2019) found that α-tubulin is modified by UbK63 chains and not UbK48 chain upon ciliary
260 disassembly and the ubiquitin ligases that have been associated with ciliary clearance of Patched
261 1 and of PDGFRαα specifically assemble UbK63 chains (Kim et al., 2015; Yue et al., 2014;
262 Schmid et al., 2018). The recognition of UbK63 chains within the cilium contrasts with the role

263 of UbK63 chains attached to signaling receptors at the plasma membrane. In the latter case,
264 UbK63 chains are not required for sorting events at the plasma membrane but UbK63 chains
265 become increasingly necessary as cargoes progress along the degradative route. At the terminal
266 step of cargo sorting into the lumen of multivesicular endosomes, a strict requirement for K63-
267 linked ubiquitin chain is observed (Shields and Piper, 2011; Stringer and Piper, 2011; Huang et
268 al., 2013).

269 The contrast between sites of action of molecular regulators extends to β arrestin-directed
270 ubiquitination. While β arrestin functions in cilia to direct the addition of ubiquitin onto
271 activated GPCRs (**Figure 4**), β arrestin-mediated ubiquitination of plasma membrane GPCRs
272 selectively affects sorting at the level of endosomes rather that at the plasma membrane
273 (Bhandari et al., 2007; Henry et al., 2012; Shenoy et al., 2008). In this context, the recognition of
274 K63-linked ubiquitin chain inside cilia may befit the endosomal origin of primary cilia (Sorokin,
275 1962; Westlake et al., 2011; Mitchell, 2017).

276 Finally, an interesting consideration is the relationship between ciliary exit and endocytosis. It has
277 been proposed that endocytosis of signaling receptors is intimately coupled to their exit from cilia
278 (Pedersen et al., 2016). However, single molecule imaging of GPR161 exiting cilia suggests that
279 activated GPR161 diffuses into the plasma membrane after its exit from the ciliary compartment
280 (Ye et al., 2018). Prior findings of translational ubiquitin fusion with ciliary proteins accumulating
281 in cilia of nematodes mutants for BBSome or the ESCRT machinery (Hu et al., 2007; Xu et al.,
282 2015) suggest the provocative possibility that ciliary exit may be directly coupled to degradative
283 sorting and more work will be require to determine the route taken by ubiquitinated GPCRs out
284 of cilia.

285

286 **Ubiquitination and control of the ciliary proteome**

287 A role for ubiquitination in selecting unwanted proteins for removal from cilia may unify the
288 functions of the BBSome in signal-dependent retrieval of GPCRs and the constitutive clearance
289 of proteins that accidentally enter cilia. In both of these cases, unwanted ciliary proteins need to

290 be recognized as 'non-self' by a ciliary surveillance machinery. For GPCRs, β arrestin orchestrate
291 the recognition of activated GPCRs as unwanted by directing their ubiquitination. A fascinating
292 question for future investigations is how the more than 100 proteins that accumulate in outer
293 segments of *Bbs* photoreceptors are recognized as 'non-self' and tagged with ubiquitin.
294

295 **REFERENCES**

296 Anvarian, Z., K. Mykytyn, S. Mukhopadhyay, L.B. Pedersen, and S.T. Christensen. 2019.
297 Cellular signalling by primary cilia in development, organ function and disease. *Nat. Rev.*
298 *Nephrol.* doi:10.1038/s41581-019-0116-9.

299 Baker, S.A., M. Haeri, P. Yoo, S.M. Gospe, N.P. Skiba, B.E. Knox, and V.Y. Arshavsky. 2008.
300 The outer segment serves as a default destination for the trafficking of membrane proteins
301 in photoreceptors. *J. Cell Biol.* 183:485–498. doi:10.1083/jcb.200806009.

302 Bhandari, D., J. Trejo, J.L. Benovic, and A. Marchese. 2007. Arrestin-2 interacts with the
303 ubiquitin-protein isopeptide ligase atrophin-interacting protein 4 and mediates
304 endosomal sorting of the chemokine receptor CXCR4. *J. Biol. Chem.* 282:36971–36979.
305 doi:10.1074/jbc.M705085200.

306 Chiang, A.P., J.S. Beck, H. Yen, M.K. Tayeh, T.E. Scheetz, R.E. Swiderski, D.Y. Nishimura,
307 T.A. Braun, K.-Y.A. Kim, J. Huang, K. Elbedour, R. Carmi, D.C. Slusarski, T.L.
308 Casavant, E.M. Stone, and V.C. Sheffield. 2006. Homozygosity mapping with SNP
309 arrays identifies TRIM32, an E3 ubiquitin ligase, as a Bardet-Biedl syndrome gene
310 (BBS11). *Proc. Natl. Acad. Sci. U. S. A.* 103:6287–6292. doi:10.1073/pnas.0600158103.

311 Corbit, K.C., P. Aanstad, V. Singla, A.R. Norman, D.Y.R. Stainier, and J.F. Reiter. 2005.
312 Vertebrate Smoothened functions at the primary cilium. *Nature*. 437:1018–1021.
313 doi:10.1038/nature04117.

314 Craige, B., J.M. Brown, and G.B. Witman. 2013. Isolation of Chlamydomonas Flagella. *Curr.*
315 *Protoc. Cell Biol.* 59:3.41.1-3.41.9. doi:10.1002/0471143030.cb0341s59.

316 Datta, P., C. Allamargot, J.S. Hudson, E.K. Andersen, S. Bhattarai, A.V. Drack, V.C. Sheffield,
317 and S. Seo. 2015. Accumulation of non-outer segment proteins in the outer segment
318 underlies photoreceptor degeneration in Bardet-Biedl syndrome. *Proc Natl Acad Sci U A*.
319 112:E4400–9. doi:10.1073/pnas.1510111112.

320 Domire, J.S., J.A. Green, K.G. Lee, A.D. Johnson, C.C. Askwith, and K. Mykytyn. 2011.
321 Dopamine receptor 1 localizes to neuronal cilia in a dynamic process that requires the
322 Bardet-Biedl syndrome proteins. *Cell. Mol. Life Sci. CMLS*. 68:2951–2960.
323 doi:10.1007/s00018-010-0603-4.

324 Emmerich, C.H., and P. Cohen. 2015. Optimising methods for the preservation, capture and
325 identification of ubiquitin chains and ubiquitylated proteins by immunoblotting. *Biochem.*
326 *Biophys. Res. Commun.* 466:1–14. doi:10.1016/j.bbrc.2015.08.109.

327 Fujimuro, M., H. Sawada, and H. Yokosawa. 1994. Production and characterization of
328 monoclonal antibodies specific to multi-ubiquitin chains of polyubiquitinated proteins.
329 *FEBS Lett.* 349:173–180. doi:10.1016/0014-5793(94)00647-4.

330 Gorman, D.S., and R.P. Levine. 1965. Cytochrome f and plastocyanin: their sequence in the
331 photosynthetic electron transport chain of Chlamydomonas reinhardi. *Proc. Natl. Acad. Sci.*
332 *U. S. A.* 54:1665–1669. doi:10.1073/pnas.54.6.1665.

333 Green, J.A., C.L. Schmid, E. Bley, P.C. Monsma, A. Brown, L.M. Bohn, and K. Mykytyn. 2015.
334 Recruitment of β-Arrestin into Neuronal Cilia Modulates Somatostatin Receptor
335 Subtype 3 Ciliary Localization. *Mol. Cell. Biol.* 36:223–235. doi:10.1128/MCB.00765-15.

336 Haglund, K., S. Sigismund, S. Polo, I. Szymkiewicz, P.P. Di Fiore, and I. Dikic. 2003. Multiple
337 monoubiquitination of RTKs is sufficient for their endocytosis and degradation. *Nat. Cell*
338 *Biol.* 5:461–466. doi:10.1038/ncb983.

339 Henry, A.G., J.N. Hislop, J. Grove, K. Thorn, M. Marsh, and M. von Zastrow. 2012.
340 Regulation of endocytic clathrin dynamics by cargo ubiquitination. *Dev. Cell.* 23:519–532.
341 doi:10.1016/j.devcel.2012.08.003.

342 Howarth, M., and A.Y. Ting. 2008. Imaging proteins in live mammalian cells with biotin ligase
343 and monovalent streptavidin. *Nat. Protoc.* 3:534–545. doi:10.1038/nprot.2008.20.

344 Hu, J., S.G. Wittekind, and M.M. Barr. 2007. STAM and Hrs down-regulate ciliary TRP
345 receptors. *Mol. Biol. Cell.* 18:3277–3289. doi:10.1091/mbc.E07-03-0239.

346 Huang, F., X. Zeng, W. Kim, M. Balasubramani, A. Fortian, S.P. Gygi, N.A. Yates, and A.
347 Sorkin. 2013. Lysine 63-linked polyubiquitination is required for EGF receptor
348 degradation. *Proc. Natl. Acad. Sci.* 110:15722–15727. doi:10.1073/pnas.1308014110.

349 Huang, K., D.R. Diener, and J.L. Rosenbaum. 2009. The ubiquitin conjugation system is
350 involved in the disassembly of cilia and flagella. *J. Cell Biol.* 186:601–613.
351 doi:10.1083/jcb.200903066.

352 Husnjak, K., and I. Dikic. 2012. Ubiquitin-binding proteins: decoders of ubiquitin-mediated
353 cellular functions. *Annu. Rev. Biochem.* 81:291–322. doi:10.1146/annurev-biochem-
354 051810-094654.

355 Jin, H., S.R. White, T. Shida, S. Schulz, M. Aguiar, S.P. Gygi, J.F. Bazan, and M.V. Nachury.
356 2010. The conserved Bardet-Biedl syndrome proteins assemble a coat that traffics
357 membrane proteins to cilia. *Cell.* 141:1208–1219. doi:10.1016/j.cell.2010.05.015.

358 Kim, J., E.Y. C Hsia, A. Brigui, A. Plessis, P.A. Beachy, and X. Zheng. 2015. The role of ciliary
359 trafficking in Hedgehog receptor signaling. *Sci. Signal.* 8:ra55–ra55.
360 doi:10.1126/scisignal.aaa5622.

361 Klink, B.U., E. Zent, P. Juneja, A. Kuhlee, S. Raunser, and A. Wittinghofer. 2017. A
362 recombinant BBSome core complex and how it interacts with ciliary cargo. *eLife*. 6.
363 doi:10.7554/eLife.27434.

364 Langousis, G., M.M. Shimogawa, E.A. Saada, A.A. Vashisht, R. Spreafico, A.R. Nager, W.D.
365 Barshop, M.V. Nachury, J.A. Wohlschlegel, and K.L. Hill. 2016. Loss of the BBSome
366 perturbs endocytic trafficking and disrupts virulence of Trypanosoma brucei. *Proc Natl*
367 *Acad Sci U A*. 113:632–637. doi:10.1073/pnas.1518079113.

368 Lechtreck, K.-F., E.C. Johnson, T. Sakai, D. Cochran, B.A. Ballif, J. Rush, G.J. Pazour, M.
369 Ikebe, and G.B. Witman. 2009. The Chlamydomonas reinhardtii BBSome is an IFT
370 cargo required for export of specific signaling proteins from flagella. *J. Cell Biol.*
371 187:1117–1132. doi:10.1083/jcb.200909183.

372 Liew, G.M., F. Ye, A.R. Nager, J.P. Murphy, J.S. Lee, M. Aguiar, D. Breslow, S.P. Gygi, and
373 M.V. Nachury. 2014. The intraflagellar transport protein IFT27 promotes BBSome exit
374 from cilia through the GTPase ARL6/BBS3. *Dev. Cell*. 31:265–278.
375 doi:10.1016/j.devcel.2014.09.004.

376 Loktev, A.V., and P.K. Jackson. 2013. Neuropeptide Y family receptors traffic via the Bardet-
377 Biedl syndrome pathway to signal in neuronal primary cilia. *Cell Rep.* 5:1316–1329.
378 doi:10.1016/j.celrep.2013.11.011.

379 McCullough, J., M.J. Clague, and S. Urbé. 2004. AMSH is an endosome-associated ubiquitin
380 isopeptidase. *J. Cell Biol.* 166:487–492. doi:10.1083/jcb.200401141.

381 McCullough, J., P.E. Row, Ó. Lorenzo, M. Doherty, R. Beynon, M.J. Clague, and S. Urbé.
382 2006. Activation of the Endosome-Associated Ubiquitin Isopeptidase AMSH by STAM,
383 a Component of the Multivesicular Body-Sorting Machinery. *Curr. Biol.* 16:160–165.
384 doi:10.1016/j.cub.2005.11.073.

385 Michel, M.A., P.R. Elliott, K.N. Swatek, M. Simicek, J.N. Pruneda, J.L. Wagstaff, S.M.V.
386 Freund, and D. Komander. 2015. Assembly and specific recognition of k29- and k33-
387 linked polyubiquitin. *Mol. Cell*. 58:95–109. doi:10.1016/j.molcel.2015.01.042.

388 Milenkovic, L., L.E. Weiss, J. Yoon, T.L. Roth, Y.S. Su, S.J. Sahl, M.P. Scott, and W.E.
389 Moerner. 2015. Single-molecule imaging of Hedgehog pathway protein Smoothened in
390 primary cilia reveals binding events regulated by Patched1. *Proc Natl Acad Sci U A*.
391 112:8320–8325. doi:10.1073/pnas.1510094112.

392 Mitchell, D.R. 2017. Evolution of Cilia. *Cold Spring Harb. Perspect. Biol.* 9:a028290.
393 doi:10.1101/cshperspect.a028290.

394 Mukhopadhyay, S., X. Wen, N. Ratti, A. Loktev, L. Rangell, S.J. Scales, and P.K. Jackson.
395 2013. The ciliary G-protein-coupled receptor Gpr161 negatively regulates the Sonic
396 hedgehog pathway via cAMP signaling. *Cell.* 152:210–223.
397 doi:10.1016/j.cell.2012.12.026.

398 Mykytyn, K., and C. Askwith. 2017. G-Protein-Coupled Receptor Signaling in Cilia. *Cold Spring*
399 *Harb. Perspect. Biol.* a028183. doi:10.1101/cshperspect.a028183.

400 Mykytyn, K., R.F. Mullins, R.F. Mullins, M. Andrews, M. Andrews, A.P. Chiang, A.P. Chiang,
401 R.E. Swiderski, R.E. Swiderski, B. Yang, B. Yang, T. Braun, T. Braun, T. Casavant, T.
402 Casavant, E.M. Stone, E.M. Stone, and V.C. Sheffield. 2004. Bardet-Biedl syndrome
403 type 4 (BBS4)-null mice implicate Bbs4 in flagella formation but not global cilia assembly.
404 *Proc. Natl. Acad. Sci. U. S. A.* 101:8664–8669. doi:10.1073/pnas.0402354101.

405 Nachury, M.V. 2018. The molecular machines that traffic signaling receptors into and out of
406 cilia. *Curr. Opin. Cell Biol.* 51:124–131. doi:10.1016/j.ceb.2018.03.004.

407 Nachury, M.V., and D.U. Mick. 2019. Establishing and regulating the composition of cilia for
408 signal transduction. *Nat. Rev. Mol. Cell Biol.* 20:389–405. doi:10.1038/s41580-019-0116-4.

409 Nager, A.R., J.S. Goldstein, V. Herranz-Pérez, D. Portran, F. Ye, J.M. García-Verdugo, and
410 M.V. Nachury. 2017. An Actin Network Dispatches Ciliary GPCRs into Extracellular
411 Vesicles to Modulate Signaling. *Cell.* 168:252–263.e14. doi:10.1016/j.cell.2016.11.036.

412 Nakata, K., D. Shiba, D. Kobayashi, and T. Yokoyama. 2012. Targeting of Nphp3 to the
413 primary cilia is controlled by an N-terminal myristoylation site and coiled-coil domains.
414 *Cytoskelet. Hoboken NJ.* 69:221–234. doi:10.1002/cm.21014.

415 Newton, K., M.L. Matsumoto, I.E. Wertz, D.S. Kirkpatrick, J.R. Lill, J. Tan, D. Dugger, N.
416 Gordon, S.S. Sidhu, F.A. Fellouse, L. Komuves, D.M. French, R.E. Ferrando, C. Lam,
417 D. Compaan, C. Yu, I. Bosanac, S.G. Hymowitz, R.F. Kelley, and V.M. Dixit. 2008.
418 Ubiquitin chain editing revealed by polyubiquitin linkage-specific antibodies. *Cell.*
419 134:668–678. doi:10.1016/j.cell.2008.07.039.

420 Pal, K., S. Hwang, B. Somatilaka, H. Badgandi, P.K. Jackson, K. DeFea, and S.
421 Mukhopadhyay. 2016. Smoothened determines β-arrestin-mediated removal of the G
422 protein-coupled receptor Gpr161 from the primary cilium. *J. Cell Biol.* 212:861–875.
423 doi:10.1083/jcb.201506132.

424 Pedersen, L.B., J.B. Mogensen, and S.T. Christensen. 2016. Endocytic Control of Cellular
425 Signaling at the Primary Cilium. *Trends Biochem. Sci.* 41:784–797.
426 doi:10.1016/j.tibs.2016.06.002.

427 Rohatgi, R., L. Milenkovic, and M.P. Scott. 2007. Patched1 regulates hedgehog signaling at the
428 primary cilium. *Sci. N. Y. NY.* 317:372–376. doi:10.1126/science.1139740.

429 Sato, Y., A. Yoshikawa, A. Yamagata, H. Mimura, M. Yamashita, K. Ookata, O. Nureki, K.
430 Iwai, M. Komada, and S. Fukai. 2008. Structural basis for specific cleavage of Lys 63-
431 linked polyubiquitin chains. *Nature.* 455:358–362. doi:10.1038/nature07254.

432 Schmid, F.M., K.B. Schou, M.J. Vilhelm, M.S. Holm, L. Breslin, P. Farinelli, L.A. Larsen, J.S.
433 Andersen, L.B. Pedersen, and S.T. Christensen. 2018. IFT20 modulates ciliary PDGFRα
434 signaling by regulating the stability of Cbl E3 ubiquitin ligases. *J. Cell Biol.* 217:151–161.
435 doi:10.1083/jcb.201611050.

436 Seo, S., Q. Zhang, K. Bugge, D. Breslow, C.C. Searby, M.V. Nachury, and V.C. Sheffield.
437 2011. A novel protein LZTFL1 regulates ciliary trafficking of the BBSome and
438 Smoothened. *PLoS Genet.* 7:e1002358. doi:10.1371/journal.pgen.1002358.

439 Shaner, N.C., G.G. Lambert, A. Chammas, Y. Ni, P.J. Cranfill, M.A. Baird, B.R. Sell, J.R.
440 Allen, R.N. Day, M. Israelsson, M.W. Davidson, and J. Wang. 2013. A bright
441 monomeric green fluorescent protein derived from Branchiostoma lanceolatum. *Nat.*
442 *Methods.* 10:407–409. doi:10.1038/nmeth.2413.

443 Shankar, H., H. Shankar, A. Michal, A. Michal, R.C. Kern, R.C. Kern, D.S. Kang, D.S. Kang,
444 V.V. Gurevich, V.V. Gurevich, and J.L. Benovic. 2010. Non-visual arrestins are
445 constitutively associated with the centrosome and regulate centrosome function. *J. Biol.*
446 *Chem.* 285:8316–8329. doi:10.1074/jbc.M109.062521.

447 Shearer, R.F., and D.N. Saunders. 2016. Regulation of primary cilia formation by the ubiquitin-
448 proteasome system. *Biochem. Soc. Trans.* 44:1265–1271. doi:10.1042/BST20160174.

449 Shenoy, S.K., K. Xiao, V. Venkataramanan, P.M. Snyder, N.J. Freedman, and A.M. Weissman.
450 2008. Nedd4 mediates agonist-dependent ubiquitination, lysosomal targeting, and
451 degradation of the beta2-adrenergic receptor. *J. Biol. Chem.* 283:22166–22176.
452 doi:10.1074/jbc.M709668200.

453 Shields, S.B., and R.C. Piper. 2011. How ubiquitin functions with ESCRTs. *Traffic Cph. Den.*
454 12:1306–1317. doi:10.1111/j.1600-0854.2011.01242.x.

455 Sorokin, S. 1962. Centrioles and the formation of rudimentary cilia by fibroblasts and smooth
456 muscle cells. *J. Cell Biol.* 15:363–377. doi:10.1083/jcb.15.2.363.

457 Stringer, D.K., and R.C. Piper. 2011. A single ubiquitin is sufficient for cargo protein entry into
458 MVBs in the absence of ESCRT ubiquitination. *J. Cell Biol.* 192:229–242.
459 doi:10.1083/jcb.201008121.

460 Swatek, K.N., and D. Komander. 2016. Ubiquitin modifications. *Cell Res.* 26:399–422.
461 doi:10.1038/cr.2016.39.

462 Wang, Q., Z. Peng, H. Long, X. Deng, and K. Huang. 2019. Polyubiquitylation of α-tubulin at
463 K304 is required for flagellar disassembly in Chlamydomonas. *J. Cell Sci.* 132.
464 doi:10.1242/jcs.229047.

465 Westlake, C.J., L.M. Baye, M.V. Nachury, K.J. Wright, K.E. Ervin, L. Phu, C. Chalouni, J.S.
466 Beck, D.S. Kirkpatrick, D.C. Slusarski, V.C. Sheffield, R.H. Scheller, and P.K. Jackson.
467 2011. Primary cilia membrane assembly is initiated by Rab11 and transport protein
468 particle II (TRAPPII) complex-dependent trafficking of Rabin8 to the centrosome. *Proc*
469 *Natl Acad Sci U A.* 108:2759–2764. doi:10.1073/pnas.1018823108.

470 Wingfield, J.L., K.-F. Lechtreck, and E. Lorentzen. 2018. Trafficking of ciliary membrane
471 proteins by the intraflagellar transport/BBSome machinery. *Essays Biochem.* 62:753–763.
472 doi:10.1042/EBC20180030.

473 Wright, K.J., L.M. Baye, A. Olivier-Mason, S. Mukhopadhyay, L. Sang, M. Kwong, W. Wang,
474 P.R. Pretorius, V.C. Sheffield, P. Sengupta, D.C. Slusarski, and P.K. Jackson. 2011. An
475 ARL3-UNC119-RP2 GTPase cycle targets myristoylated NPHP3 to the primary cilium.
476 *Genes Dev.* 25:2347–2360. doi:10.1101/gad.173443.111.

477 Xu, Q., Y. Zhang, Q. Wei, Y. Huang, Y. Li, K. Ling, and J. Hu. 2015. BBS4 and BBS5 show
478 functional redundancy in the BBSome to regulate the degradative sorting of ciliary
479 sensory receptors. *Sci. Rep.* 5:11855. doi:10.1038/srep11855.

480 Yau, R., and M. Rape. 2016. The increasing complexity of the ubiquitin code. *Nat. Cell Biol.*
481 18:579–586. doi:10.1038/ncb3358.

482 Ye, F., A.R. Nager, and M.V. Nachury. 2018. BBSome trains remove activated GPCRs from
483 cilia by enabling passage through the transition zone. *J. Cell Biol.* 217:1847–1868.
484 doi:10.1083/jcb.201709041.

485 Yue, S., L.-Y. Tang, Y. Tang, Y. Tang, Q.-H. Shen, J. Ding, Y. Chen, Z. Zhang, T.-T. Yu, Y.E.
486 Zhang, and S.Y. Cheng. 2014. Requirement of Smurf-mediated endocytosis of Patched1
487 in sonic hedgehog signal reception. *eLife.* 3:128. doi:10.7554/eLife.02555.

488 Zhang, Q., D. Nishimura, S. Seo, T. Vogel, D.A. Morgan, C. Searby, K. Bugge, E.M. Stone, K.
489 Rahmouni, and V.C. Sheffield. 2011. Bardet-Biedl syndrome 3 (Bbs3) knockout mouse

model reveals common BBS-associated phenotypes and Bbs3 unique phenotypes. *Proc Natl Acad Sci U A*. 108:20678–20683. doi:10.1073/pnas.1113220108.

494 **ACKNOWLEDGMENTS**

495 We thank Drs. Kirk Mykytyn, Val Sheffield, Alice Ting, and Mark Scott for the gifts of cDNAs;
496 Kathryn Anderson, Vishva Dixit (Genentech), and Felice Dunn for the gifts of antibodies; Val
497 Sheffield for the gift of the *Bbs4*$^{-/-}$ mice, George B. Witman and the Chlamydomonas Resource
498 Center for the gifs of *Chlamydomonas* strains; Yien-Ming Kuo for help with cryosections of mouse
499 retina and core support; Dhivya Kumar and Tyler Picariello for the assistance with
500 *Chlamydomonas* cultures; Nicholas Morante and Jeremy Reiter for providing *Bbs4*$^{-/-}$ mouse eyes;
501 Fan Ye for generating cell lines used in the study; Irene Ojeda Naharros for help with single cilia
502 tracking and the Nachury lab for helpful discussions. This work was funded by NIGMS (R01-
503 GM089933, M.V.N.). This work was made possible, in part, by NEI EY002162 - Core Grant for
504 Vision Research and by the Research to Prevent Blindness Unrestricted Grant (M.V.N.).
505 Authors contributions: SRS conducted all experimental work except for the experiments in
506 Figure 4A-D, which were conducted by ARN. MVN supervised research. SRS and MVN wrote
507 the manuscript.

508

509

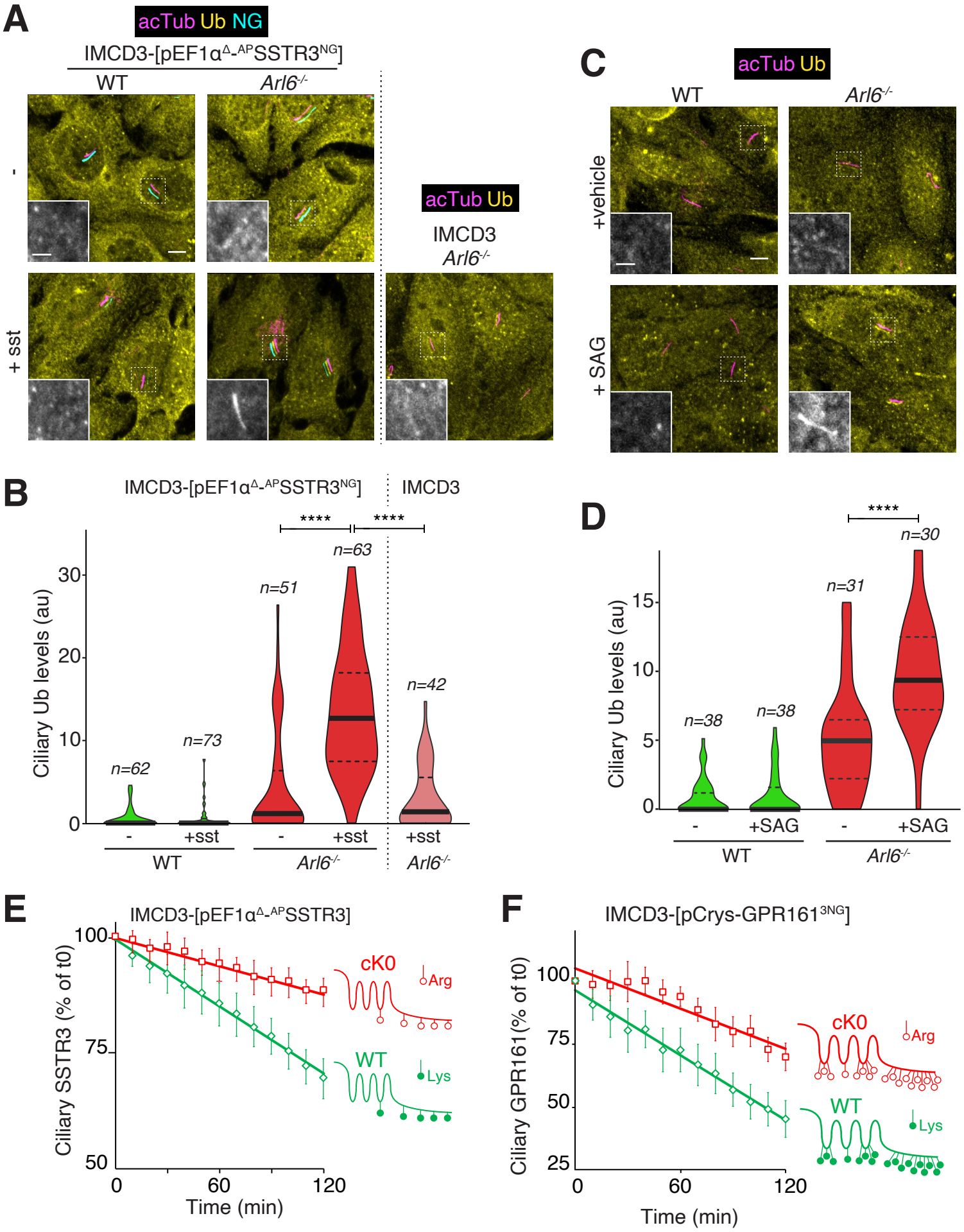
A
acTub Ub NG
IMCD3-[pEF1α$^{\Delta}$-^{AP}SSTR3^{NG}]
WT
Arl6-/-
-
+ sst
acTub Ub
IMCD3
Arl6-/-
C
acTub Ub
WT
Arl6-/-
+vehicle
+ SAG
B
IMCD3-[pEF1α$^{\Delta}$-^{AP}SSTR3^{NG}]
IMCD3
****
****
Ciliary Ub levels (au)
n=62
n=73
n=51
n=63
n=42
-
+sst
-
+sst
+sst
WT
Arl6-/-
Arl6-/-
D
****
Ciliary Ub levels (au)
n=38
n=38
n=31
n=30
-
+SAG
-
+SAG
WT
Arl6-/-
E
IMCD3-[pEF1α$^{\Delta}$-^{AP}SSTR3]
Ciliary SSTR3 (% of t0)
cK0
Arg
WT
Lys
Time (min)
F
IMCD3-[pCrys-GPR161^{3NG}]
Ciliary GPR161 (% of t0)
cK0
Arg
WT
Lys
Time (min)

Figure 1

510 **Figure 1. Signal-dependent ubiquitination of ciliary GPCRs drives their BBSome-**
511 **dependent exit.**
512 **A.** SSTR3 fused to the fluorescent protein mNeonGreen (NG) at its intracellular C-terminus and
513 a biotinylation Acceptor Peptide (AP) tag at its extracellular N-terminus was expressed under the
514 control of an attenuated EF1α promoter (pEF1α$^{\Delta}$) in wild type (WT) and *Arl6*$^{-/-}$ IMCD3 cells.
515 Cells were treated with or without somatostatin-14 (sst) for 2 h, then fixed and stained for
516 acetylated tubulin (acTub, magenta) and ubiquitin (Ub, yellow in main panels and gray in insets).
517 ^{AP}SSTR3^{NG} was imaged through the intrinsic fluorescence of NG. Channels were shifted in this
518 and all subsequent micrographs to facilitate visualization of ciliary signals. Scale bar: 5μm (main
519 panel), 2μm (inset). In WT cells, the ciliary SSTR3 signal decrease over the experimental time
520 course. In *Arl6*$^{-/-}$ cells, SSTR3 fails to exit cilia and an increase in the ciliary Ub level is detected.
521 As a control, *Arl6*$^{-/-}$ cells that did not express SSTR3-NG were tested; no increase in ciliary Ub
522 levels were observed upon addition of sst. **B.** The fluorescence intensity of the Ub channel in the
523 cilium was measured in each condition and the data are represented as violin plots. The thick bar
524 indicates the median and the dotted lines the first and third quartiles. An 11-fold increase in
525 ciliary Ub signal is observed upon addition of sst to SSTR3-expressing cells. Asterisks indicate
526 ANOVA significance value. ****, p= <0.0001. **C.** IMCD3 cells of the indicated genotypes were
527 treated with the Smoothened agonist SAG or the vehicle DMSO for 2h. Cells were then fixed
528 and stained for acTub and Ub. Scale bar 5μm (main panel), 2μm (inset). Activation of Hh
529 signaling promotes a detectable increase in ciliary Ub levels only in *Arl6*$^{-/-}$ cells. **D.** Violin plots of
530 the fluorescence intensity of the Ub channel in the cilium in each condition are shown. Asterisks
531 indicate ANOVA significance value. ****, p= <0.0001. **E.** IMCD3-[pEF1α$^{\Delta}$-^{AP}SSTR3] stably
532 expressed the ER-localized biotin ligase BirA to enables the biotinlylation of ^{AP}SSTR3. SSTR3
533 was either the wild-type allele (WT) or a variant where all five cytoplasm-facing lysine residues
534 (listed in Methods) were mutated to arginine (cK0). Ciliary ^{AP}SSTR3 was pulse-labeled by
535 addition of Alexa647-conjugated mSA (mSA647) to the medium for 5-10 min before addition of
536 sst. Far red fluorescence was tracked in individual cilia at 10 min capture intervals. For each
537 individual cilia, fluorescence intensities were normalized to the value at t = 0. A comparison of

538 the ciliary levels of SSTR3 at t=0 is shown in **Fig. S2A**. Data were plotted and fitted to a line.
539 Error bars: 95% CI. N =18-22 cilia. **F.** GPR161 fused to three tandem repeats of NG at its C-
540 terminus was expressed under the control of the ultra-weak δ-crystallin promoter (pCrys) in
541 IMCD3 cells. GPR161 was either the wild-type allele (WT) or a variant where all eighteen
542 cytoplasm-facing lysine residues (listed in Methods) where mutated to arginine (cK0). IMCD3-
543 [pCrys-GPR161^{3NG}] cells were treated with SAG for 2h. During the course of the experiment,
544 NG fluorescence was tracked in individual cilia at 10 min capture intervals. Fluorescence data
545 were acquired and analyzed as in panel **(E)**. A comparison of the ciliary levels of GPR161 at t=0
546 is shown in **Fig. S2B**. Error bars: 95% CI. N =19-10 cilia.

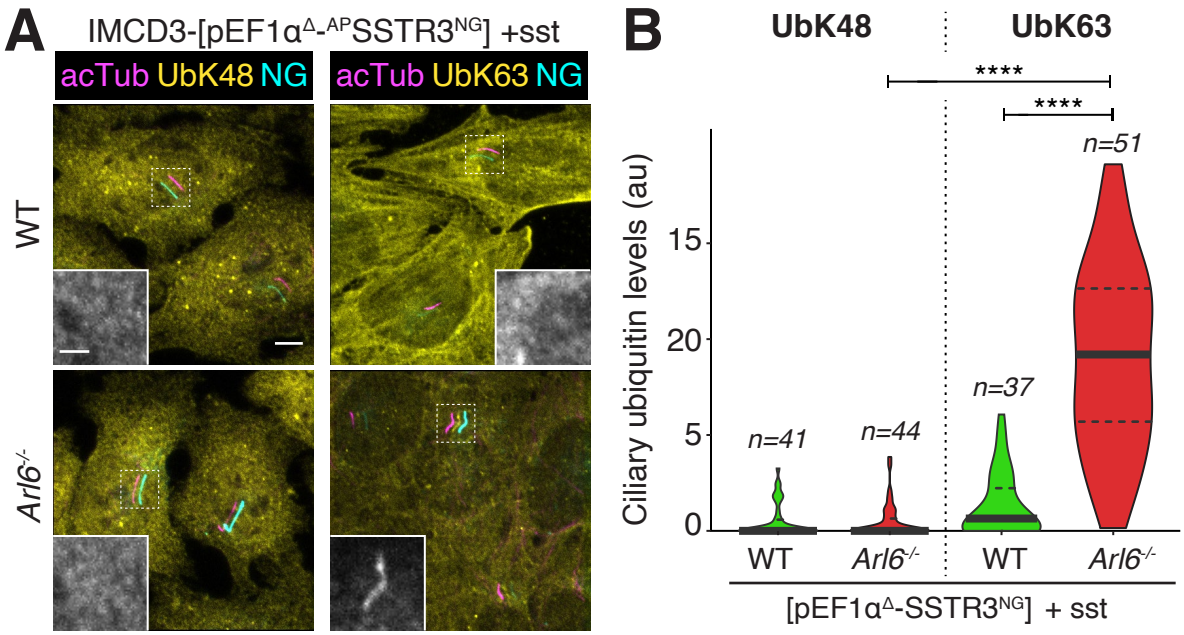
A
IMCD3-[pEF1α$^{\Delta}$-^{AP}SSTR3^{NG}] +sst
acTub UbK48 NG
acTub UbK63 NG
WT
Arl6$^{-/-}$
B
UbK48
UbK63
****
****
Ciliary ubiquitin levels (au)
0
5
15
20
n=41
n=44
n=37
n=51
WT
Arl6$^{-/-}$
WT
Arl6$^{-/-}$
[pEF1α$^{\Delta}$-SSTR3^{NG}] + sst

Figure 2

547 **Figure 2. Signal-dependent accumulation of K63-linked ubiquitin chains inside**
548 **cilia of *Bbs* mutant cells.**
549 **A.** IMCD3 cells of the indicated genotypes expressing $SSTR3^{NG}$ were treated with somatostatin-
550 14 for 2 h. Cells were fixed and stained for AcTub (magenta) and with antibodies specific for the
551 lysine 63 (UbK63) or lysine 48 (UbK48) Ub chain linkages (yellow in main panel and gray in
552 inset). $SSTR3^{NG}$ was imaged through the intrinsic fluorescence of NG. Scale bar 5μm (main
553 panel), 2μm (inset). **B.** The fluorescence intensity of the UbK48 and UbK63 channels in the
554 cilium are represented as violin plots. A 14-fold increase in ciliary Ub abundance is detected with
555 the K63Ub linkage-specific antibody. Asterisks indicate ANOVA significance value. ****, p=
556 <0.0001. No ciliary signal is detected with the K48Ub linkage-specific antibody.

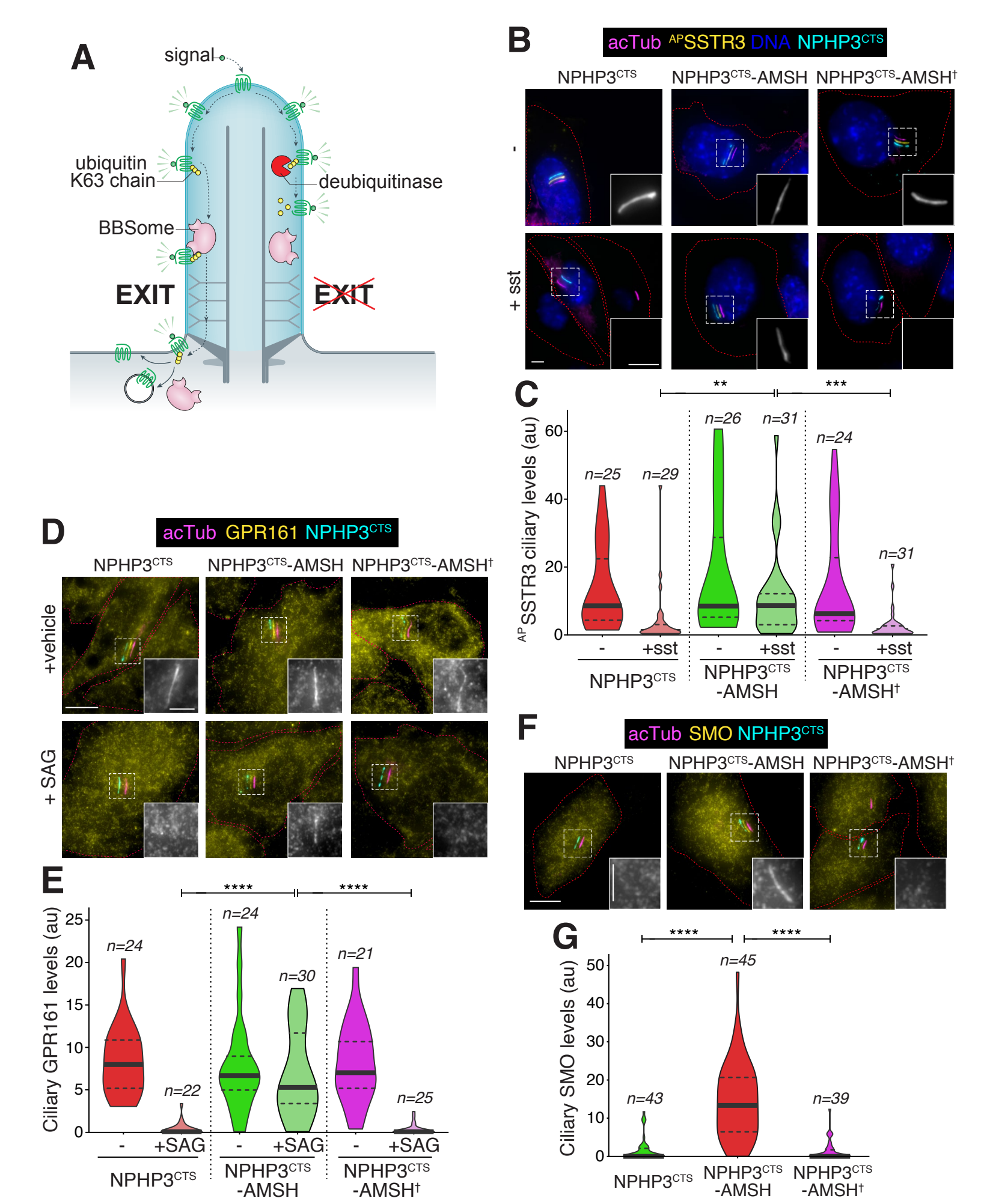
A
signal
ubiquitin
K63 chain
deubiquitinase
BBSome
EXIT
EXIT
B
acTub APSSTR3 DNA NPHP3CTS
NPHP3CTS
NPHP3CTS-AMSH
NPHP3CTS-AMSH†
-
+ sst
C
APSSTR3 ciliary levels (au)
n=25
n=29
n=26
n=31
n=24
n=31
**
***
-
+sst
NPHP3CTS
NPHP3CTS -AMSH
NPHP3CTS -AMSH†
D
acTub GPR161 NPHP3CTS
NPHP3CTS
NPHP3CTS-AMSH
NPHP3CTS-AMSH†
+vehicle
+ SAG
E
Ciliary GPR161 levels (au)
n=24
n=22
n=24
n=30
n=21
n=25
****
****
-
+SAG
NPHP3CTS
NPHP3CTS -AMSH
NPHP3CTS -AMSH†
F
acTub SMO NPHP3CTS
NPHP3CTS
NPHP3CTS-AMSH
NPHP3CTS-AMSH†
G
Ciliary SMO levels (au)
n=43
n=45
n=39
****
****
NPHP3CTS
NPHP3CTS -AMSH
NPHP3CTS -AMSH†

Figure 3

557 **Figure 3. Ciliary K63-linked ubiquitin chains are required for the removal of**
558 **BBSome cargoes from cilia.**
559 **A.** Diagram of the working model and the experimental strategy. **B.** IMCD3-[pEF1α$^{\Delta}$-
560 ^{AP}SSTR3; pEF1α-BirA•ER] were transfected with plasmids expressing the ciliary targeting signal
561 (CTS) of NPHP3 fused to GFP only (left panels), to GFP and the catalytic domain of the K63-
562 specific deubiquitinase AMSH (middle panels), or to GFP and the catalytically inactive E280A
563 variant of AMSH catalytic domain (AMSH†, right panels). Ciliary ^{AP}SSTR3 was pulse-labeled
564 with mSA647 for 5-10 min and cells were then treated with or without sst for 2h, before fixation
565 and staining for acetylated tubulin (acTub, magenta) and DNA (blue). The NPHP3^{CTS} fusions
566 were visualized through the intrinsic fluorescence of GFP (cyan) and ^{AP}SSTR3 was visualized via
567 mSA647 (yellow in the main frames and gray in the insets). Scale bar 5μm (main panel), 2μm
568 (inset). **C.** The fluorescence intensities of ciliary $^{mSA647\text{-}AP}$SSTR3 are represented as violin plots.
569 Asterisks indicate Kruskal-Wallis test significance values. ***, p= <0.001; **, p= <0.01. Addition
570 of sst triggers the exit of SSTR3 from cilia in cells transfected with the controls NPHP3^{CTS} and
571 NPHP3^{CTS}-AMSH† but NPHP3^{CTS}-AMSH blocks ciliary exit of SSTR3. **D.** RPE1-hTERT
572 (RPE) cells transfected with the indicated constructs were treated with SAG or vehicle (DMSO)
573 for 2h, then fixed and stained for acetylated tubulin (magenta) and GPR161 (yellow in the main
574 frames and gray in the insets). The NPHP3^{CTS} fusions were visualized through the intrinsic
575 fluorescence of GFP (cyan). Scale bar 5μm (main panel), 2μm (inset). **E.** The fluorescence
576 intensities of ciliary GPR161 are represented as violin plots. Asterisks indicate ANOVA
577 significance value. ****, p= <0.0001. NPHP3^{CTS}-AMSH specifically blocks the SAG-dependent
578 exit of GPR161 from cilia. **F.** IMCD3 cells transfected with the indicated constructs were fixed
579 and stained for acetylated tubulin (magenta) and SMO (yellow in the main frames and gray in
580 the insets). The NPHP3^{CTS} fusions were visualized through the intrinsic fluorescence of GFP
581 (cyan). **G.** The fluorescence intensities of ciliary SMO are represented as violin plots. Asterisks
582 indicate ANOVA significance value. ****, p= <0.0001. NPHP3^{CTS}-AMSH specifically blocks the
583 constitutive exit of SMO from cilia and promotes accumulation of SMO in cilia in the absence of
584 pathway activation.

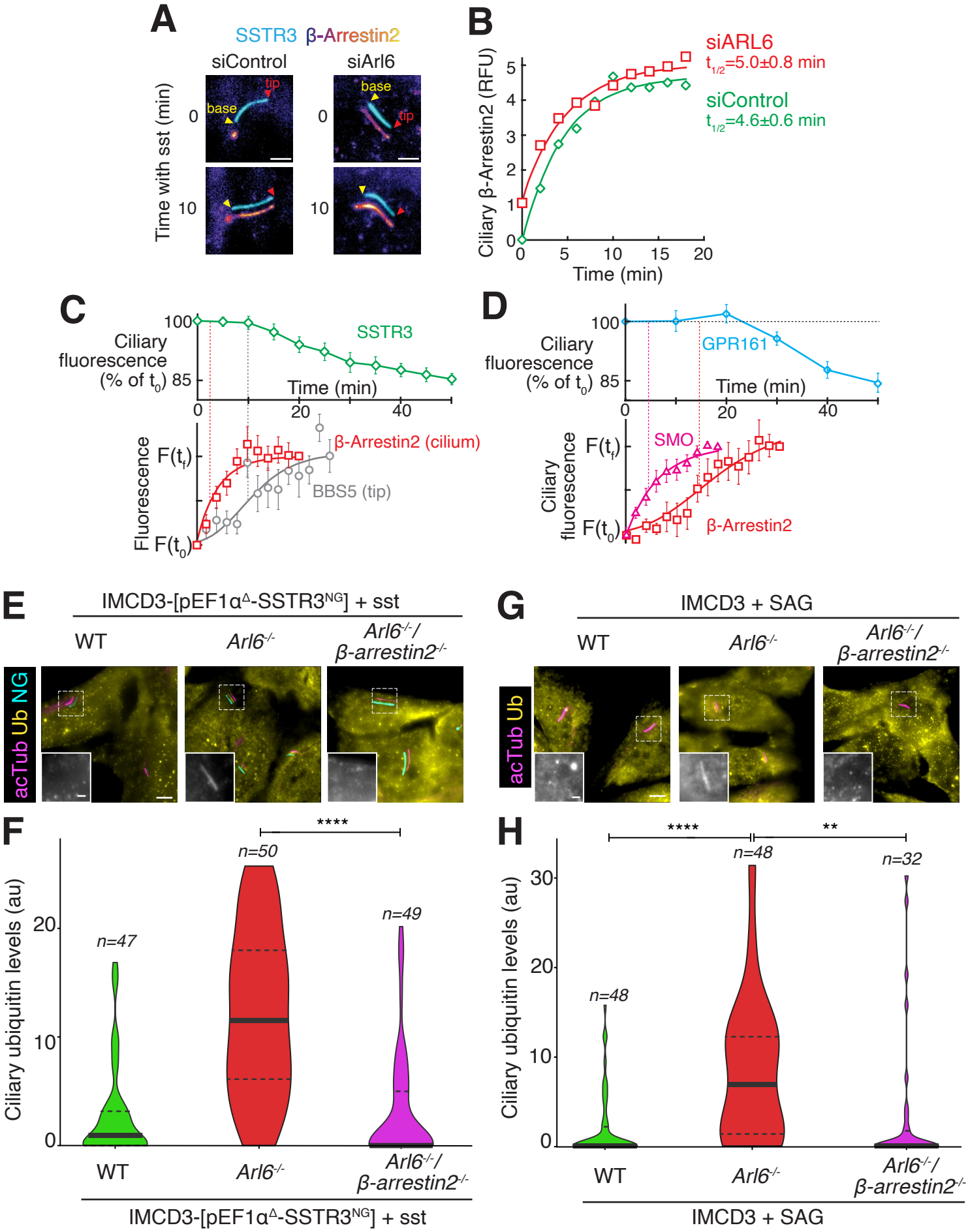
A
SSTR3 β-Arrestin2
siControl
siArl6
Time with sst (min)
0
10
base
tip
B
siARL6
t1/2=5.0±0.8 min
siControl
t1/2=4.6±0.6 min
Ciliary β-Arrestin2 (RFU)
Time (min)
C
SSTR3
Ciliary fluorescence (% of t0)
Time (min)
β-Arrestin2 (cilium)
BBS5 (tip)
Fluorescence
F(tf)
F(t0)
D
GPR161
Ciliary fluorescence (% of t0)
Time (min)
SMO
β-Arrestin2
Ciliary fluorescence
E
IMCD3-[pEF1αΔ-SSTR3NG] + sst
WT
Arl6-/-
Arl6-/- / β-arrestin2-/-
acTub Ub NG
F
Ciliary ubiquitin levels (au)
n=47
n=50
n=49
****
IMCD3-[pEF1αΔ-SSTR3NG] + sst
G
IMCD3 + SAG
acTub Ub
H
n=48
n=48
n=32
****
**
IMCD3 + SAG

Figure 4

585 **Figure 4. β-arrestin 2 directs signal-dependent ubiquitination of ciliary GPCRs.**

586 **A.** β-Arrestin2 is rapidly recruited to cilia upon activation of SSTR3. siRNA-treated IMCD3-
587 [^{AP}SSTR3, β-Arrestin2^{GFP}] cells were pulse-labeled with mSA647 before addition of sst. As
588 shown previously (Shankar et al., 2010), β-Arrestin2 is at the basal body in unstimulated cells.
589 Scale bar: 2 µm. **B.** Kinetics of β-Arrestin2^{GFP} recruitment to cilia upon sst stimulation in
590 control- and ARL6-depleted IMCD3-[^{AP}SSTR3, β-Arrestin2^{GFP}] cells. Data were fit to a simple
591 exponential. (n=10 cilia). **C-D.** Kinetics of early trafficking events for retrieval of SSTR3 (**C**)
592 and GPR161 (**D**). The top panels show removal of stably expressed ^{AP}SSTR3^{NG} or
593 ^{AP}GPR161^{NG3} following addition of sst (**C**) or SAG (**D**). The bottom panels show the kinetics of
594 β-Arrestin2^{GFP} entry (**C-D**), ^{AP}Smoothened^{NG} entry (**D**), and ^{NG3}BBS5 tip accumulation (**C**)
595 measured in IMCD3 cells stably expressing the indicated proteins. Fluorescence values are
596 normalized to the initial (t_0) and final (t_f) values. Error bars: SEM. (n=6-11 cilia). **E.** IMCD3-
597 [pEF1α$^{\Delta}$-^{AP}SSTR3^{NG}] WT, knockout for *Arl6* only and double knockout for *Arl6* and *β-Arrestin2*
598 were treated with sst for 2h before fixation and staining for acetylated tubulin (acTub, magenta)
599 and ubiquitin (Ub, yellow in the main frames and gray in the insets). SSTR3^{NG} was visualized
600 through the intrinsic fluorescence of NG. SSTR3 exit is blocked in *Arl6*$^{-/-}$ cells regardless of the *β-*
601 *Arrestin2* genotype but the ciliary Ub signal is only detected in *Arl6*$^{-/-}$ cells when β-Arrestin2
602 function is intact. Scale bar: 5µm (main panel), 1µm (inset). **F.** Violin plots representing the
603 ciliary levels of Ub under the indicated conditions. Asterisks indicate ANOVA significance value.
604 ****, p= <0.0001. **G.** IMCD3 of the indicated genotypes were treated with SAG for 2h before
605 fixation and staining for acetylated tubulin (acTub, magenta) and ubiquitin (Ub, yellow in the
606 main frames and gray in the insets). Scale bar: 5µm (main panel), 1µm (inset). **H.** Violin plots
607 representing the ciliary Ub levels. Asterisks indicate ANOVA significance value. ****, p=
608 <0.0001; **, p= <0.01. The appearance of a Ub signal in cilia in *Arl6*$^{-/-}$ cells depends on β-
609 Arrestin2.

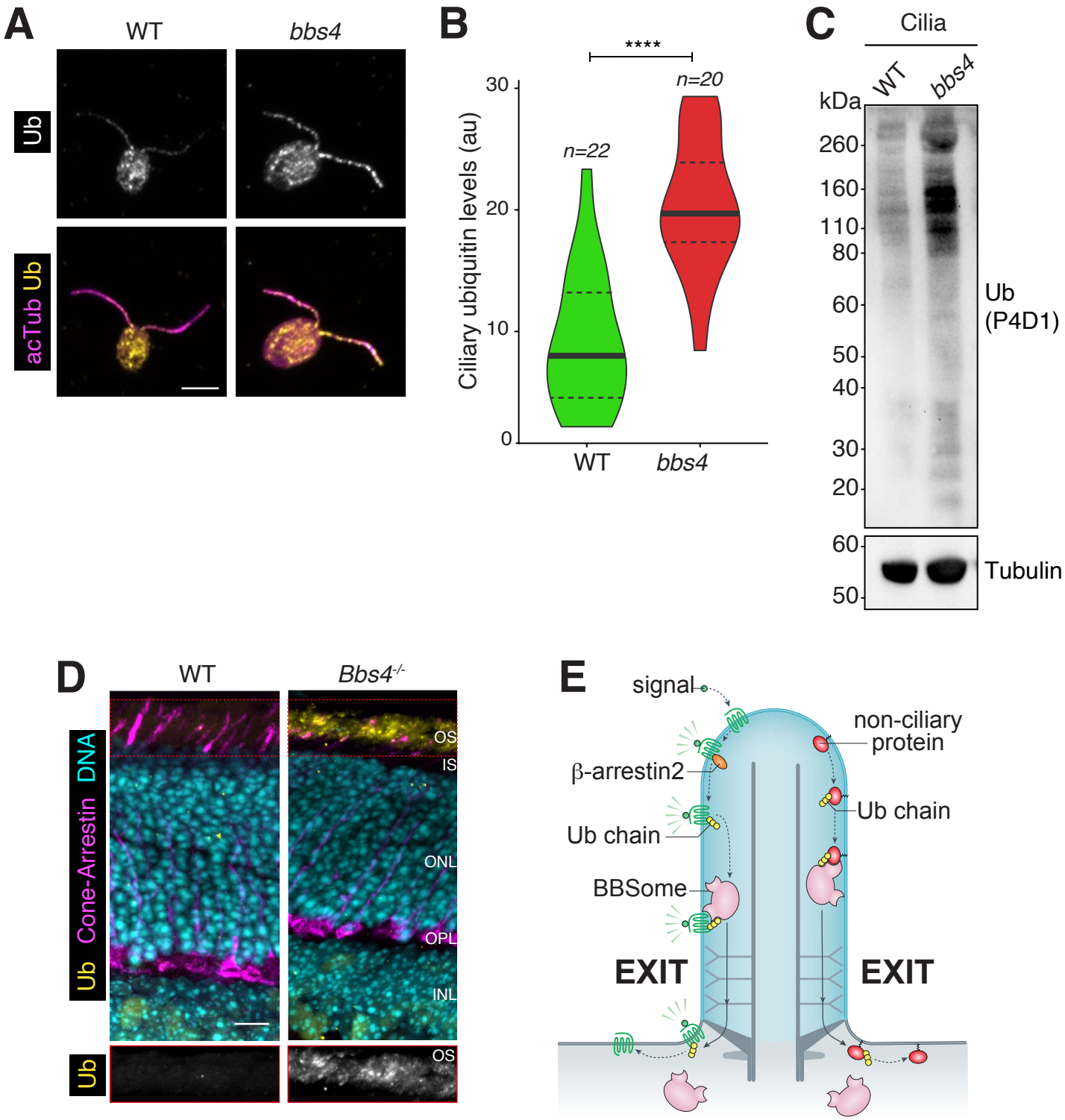
A
WT
bbs4
Ub
acTub Ub
B
****
n=22
n=20
Ciliary ubiquitin levels (au)
30
20
10
0
WT
bbs4
C
Cilia
WT
bbs4
kDa
260
160
110
80
60
50
40
30
20
Ub
(P4D1)
60
50
Tubulin
D
WT
Bbs4-/-
Ub Cone-Arrestin DNA
OS
IS
ONL
OPL
INL
Ub
OS
E
signal
non-ciliary
protein
β-arrestin2
Ub chain
Ub chain
BBSome
EXIT
EXIT

Figure 5

610 **Figure 5. Accumulation of ubiquitinated proteins in cilia of *Chlamydomonas* cells**
611 **and mammalian photoreceptors.**
612 **A.** *Chlamydomonas* cells of the indicated genotypes were fixed and stained for acetylated tubulin
613 (acTub, magenta) and ubiquitin (Ub, yellow). Scale bar: 5 µm. A weak ubiquitin signal detected
614 in WT cells is increased in *bbs4* mutant cells. **B.** Violin plots of the ciliary Ub levels in WT and
615 *bbs4 Chlamydomonas* cells. Asterisks indicate Mann-Whitney test significance values. ****, p=
616 <0.0001. The ciliary levels of Ub are increased more than 2-fold in *bbs4* cells as compared to
617 WT. **C.** Cilia purified from WT and *bbs4* cells via deciliation with dibucaine and differential
618 centrifugation were solubilized, and the protein contents resolved by SDS-PAGE. Immunoblots
619 for Ub (using the P4D1 antibody) and tubulin are shown. A rise in ubiquitin conjugates is
620 observed in *bbs4 Chlamydomonas* cells compared to WT. **D.** Mouse retina were fixed, embedded
621 and sectioned before staining for ubiquitin (Ub, yellow), cone arrestin (a marker of the
622 photoreceptor outer segment layer) and DNA (cyan). OS: outer segment; IS: inner segment;
623 ONL: outer nuclear layer; OPL: outer plexiform layer; INL: inner nuclear layer. Scale bar:
624 10µm. **E.** Model for the role of ubiquitin chains in selecting cargoes for signal-dependent and
625 constitutive exit via BBSome-mediated transport.
626
627

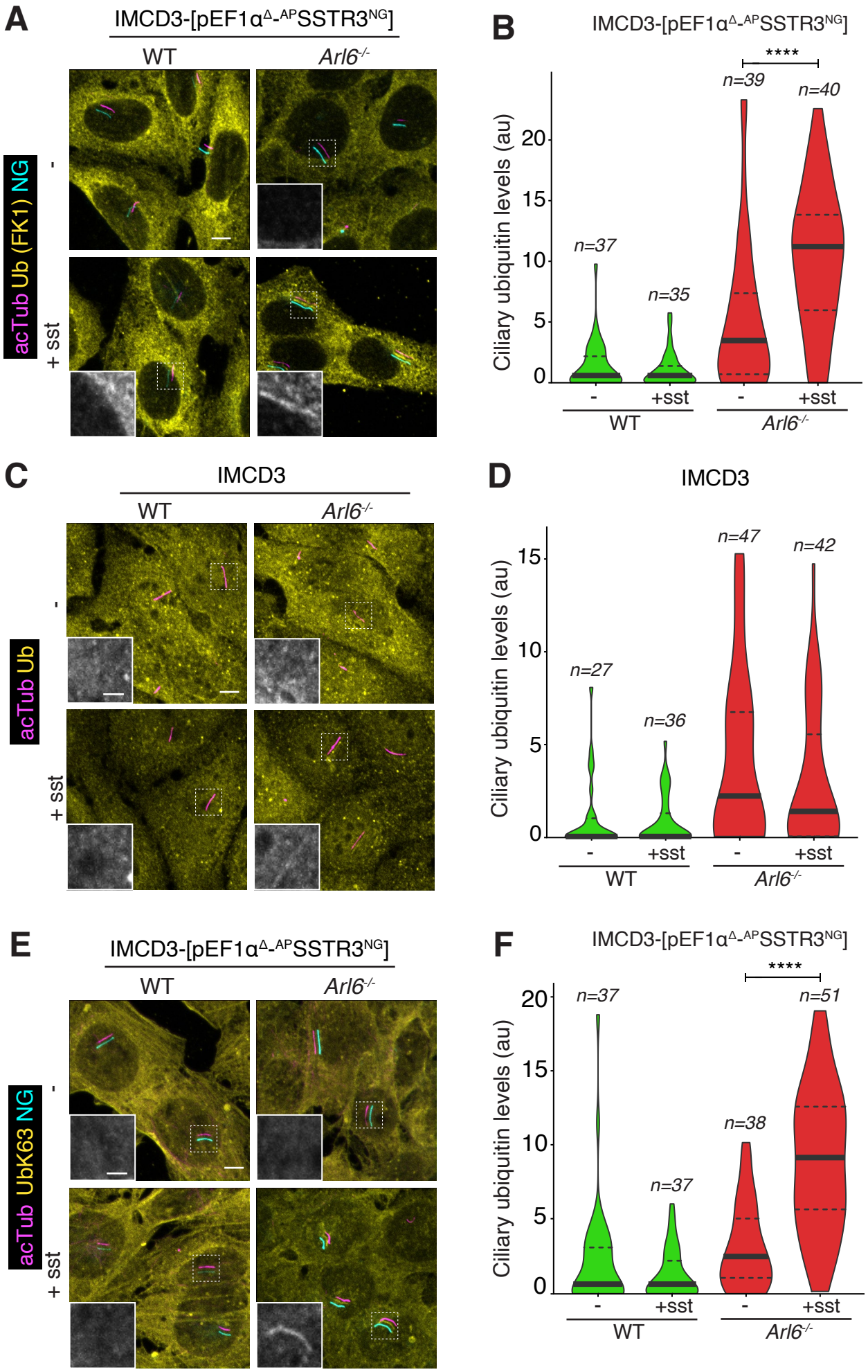

Supplementary Figure 1

628 **Figure S1. Signal-dependent ubiquitination of ciliary GPCRs**

629 **A.** IMCD3 cells of the indicated genotypes expressing ^{AP}SSTR3^{NG} were treated with
630 somatostatin (sst) for 2 h. Cells were fixed and stained for ubiquitin with the FK1 monoclonal
631 antibody (Ub (FK1), yellow in main panels and gray in insets) and acetylated tubulin (acTub,
632 magenta). ^{AP}SSTR3^{NG} was imaged through the intrinsic fluorescence of NG. Scale bar: 5µm
633 (main panel), 2µm (inset). **B.** Violin plots of the fluorescence intensity of the Ub channel in the
634 cilium in each condition are shown. A 3-fold increase in ciliary Ub signal is observed upon
635 addition of sst to SSTR3-expressing cells. Asterisks indicate ANOVA significance value. ****, p=
636 <0.0001. **C.** IMCD3 cells of the indicated genotypes were treated with or without somatostatin
637 for 2 h. Cells were fixed and stained for acetylated tubulin (acTub, magenta) and ubiquitin (Ub,
638 yellow in main panels and gray in insets). Scale bar 5µm (main panel), 2µm (inset). No significant
639 increase in ciliary Ub levels were observed upon addition of sst to *Arl6*$^{-/-}$ cells. **D.** The
640 fluorescence intensity of the Ub channel in the cilium was measured in each condition and the
641 data are represented as violin plots. **E.** IMCD3 cells of the indicated genotypes expressing
642 ^{AP}SSTR3^{NG} were treated with somatostatin-14 for 2 h. Cells were fixed and stained for AcTub
643 (magenta) and UbK63 (yellow in main panel and gray in inset). ^{AP}SSTR3^{NG} was imaged through
644 the intrinsic fluorescence of NG. Scale bar 5µm (main panel), 2µm (inset). **F.** The fluorescence
645 intensity of the UbK63 channel in the cilium is represented as violin plots. Asterisks indicate
646 ANOVA significance value. ****, p= <0.0001.

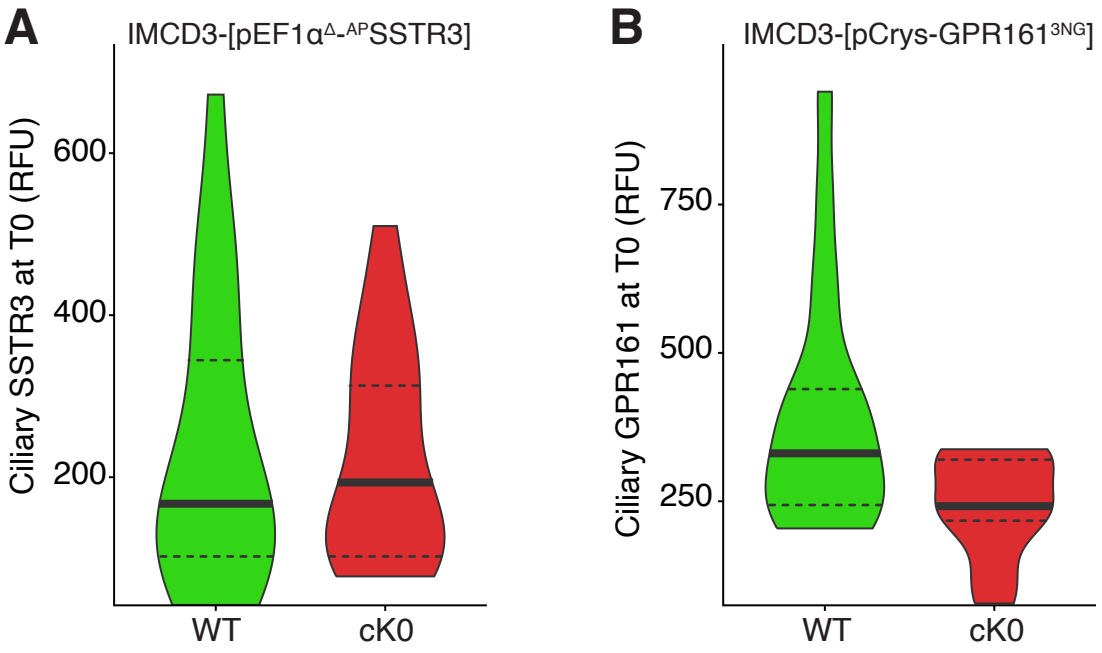

Supplementary Figure 2

647 **Figure S2. Fluorescence intensities of WT and cK0 GPCR variants at t=0.**

648 **A.** Ciliary ^{AP}SSTR3 was pulse-labeled by addition of Alexa647-conjugated mSA (mSA647) to the
649 medium for 5-10 min before addition of sst. Violin plots of the fluorescence intensities for WT
650 and cK0 SSTR3 imaged in the far red channel at t=0 are shown. **B.** Violin plots of the
651 fluorescence intensities of NG fluorescence corresponding to WT and cK0 GPR161^{NG} at t=0 are
652 shown.

653 **MATERIALS AND METHODS**

654 **Cell culture**

655 The mouse IMCD3 cell lines used in the study were generated from a parental IMCD3-FlpIn
656 cell line (gift from P.K. Jackson, Stanford University, Stanford, CA). IMCD3-FlpIn cells were
657 cultured in DMEM/F12 (11330-057; Gibco) supplemented with 10% FBS (100-106; Gemini
658 Bio-products), 100 U/ml penicillin-streptomycin (400-109; Gemini Bio-products), and 2 mM L-
659 glutamine (400-106; Gemini Bio-products). The RPE1-hTERT cell line (ATCC CRL-4000) was
660 cultured in DMEM/F12 supplemented with 10% FBS, 100 U/ml penicillin-streptomycin, 2 mM
661 L-glutamine and 0.26% sodium bicarbonate (25080; Gibco).

662 Ciliation was induced by serum starvation in media containing 0.2% FBS for 16 to 24 h.

663

664 **Plasmid construction and Generation of stable cell lines**

665 Stable isogenic IMCD3 cell lines were generated using the Flp-In system (ThermoFisher
666 Scientific). Low-expression promoters and additional expression cassettes were introduced into
667 pEF5/FRT plasmid as described (Nager et al., 2017; Ye et al., 2018). To reduce expression
668 levels, the EF1α promoter was attenuated by mutating the TATA-box (pEF1α$^{\Delta}$) or replaced with
669 a minimal chicken lens δ-crystallin promoter (pCrys).

670 Coding sequences were amplified from plasmids encoding mouse GPR161 (BC028163;
671 Mammalian Gene Collection [MGC]; GE Healthcare), mouse SSTR3 (gift from Kirk Mykytyn,
672 Ohio State University, Columbus, OH), and human BBS5 (gifts from V. Sheffield, University of
673 Iowa, Iowa City, IA), BirA-ER (gift from Alice Ting). β-arrestin 2 (a gift from Mark Scott) was
674 stably expressed from a pCMV-based plasmid (pEGFP-N). SSTR3 and SMO expression were
675 driven by pEF1α$^{\Delta}$, GPR161 expression by pCrys, and BBS5 expression by pEF1α. Coding
676 sequences were fused to GFP, mNeonGreen (NG, (Shaner et al., 2013), or an acceptor peptide
677 for the biotin ligase BirA (AP) (Howarth and Ting, 2008). Multiple rounds of site-directed
678 mutagenesis were performed to generate SSTR3-cK0, a variant with all the cytoplasm-facing

679 lysine residues (K233, K330, K356, K407, and K421) mutated to arginine. GPR161-cK0, a
680 variant with 18 cytoplasm-exposed lysine residues (K83, K84, K93, K167, K247, K250, K269,
681 K296, K358, K362, K455, K469, K473, K481, K486, K497, K504, and K548) mutated to
682 arginine, was gene synthesized (GenScript). Cilia-AMSH was generated by fusing the catalytic
683 domain of mouse AMSH (gift from David Komander; Addgene plasmid #66712; (Michel et al.,
684 2015) with NPHP3(1-200) and GFP to create NPHP3[1-200]-GFP-AMSH[243-424]. A
685 catalytically dead version of AMSH was generated by mutating the water-activating Glu280
686 residue to Ala (Sato et al., 2008; Huang et al., 2013).

687 CRISPR-edited *Arl6*$^{-/-}$ and *Arl6*$^{-/-}$/*Arrb2*$^{-/-}$ cell lines were described previously (Liew et al., 2014;
688 Nager et al., 2017). The genotypes are *Arl6*, NM_001347244.1:c.- 10_25del; c.3_6del; and *Arrb2*,
689 NM_001271358.1:c.1 12del;c112_113del.

690

691 **Transfection**

692 For generation of all stable cell lines except for the ones expressing β-arrestin 2^{GFP}, FRT-based
693 plasmids were reverse transfected using XtremeGene9 (Roche) into IMCD3 Flp-In cells along
694 with a plasmid encoding the Flp recombinase (pOG44) and stable transformants were selected by
695 blasticidin resistance (4 ug/ml). The transfection mixture was then added to the cells. pEGFP-N•
696 β-arrestin 2-GFP was transfected into IMCD3 cells using Lipofectamine 2000, and clones were
697 selected using neomycin resistance.

698

699 **Antibodies and drug treatments**

700 The following monoclonal antibodies were used for immunofluorescence: anti-acetylated tubulin
701 (mouse; clone 6-11B-1; Sigma-Aldrich; 1:500), anti-ubiquitin clone FK2 was used in all
702 experiments except where indicated (mouse; D058-3; Medical and Biological Laboratories;
703 1:500), anti-ubiquitin FK1 in **Fig. S1A-B** (mouse; D071-3; Medical and Biological Laboratories;
704 1:500), anti-ubiquitin Lys48 linkage (rabbit; clone Apu2; 05-1307; Millipore-Genentech; 1:500),

705 anti-ubiquitin Lys63 linkage (human; clone Apu3; a gift from Genentech; 1:500). The following
706 monoclonal antibodies were used for immunoblotting: anti-ubiquitin (mouse; clone P4D1; 3936;
707 Cell Signaling; 1:1000), anti-α tubulin (mouse; clone DM1A; MS-581-P1ABX; Thermo
708 Scientific;1:1000). The following polyclonal antibodies were used for immunofluorescence: anti-
709 GPR161 (rabbit; 13398-1-AP; Proteintech; 1:100), anti-Smoothened (rabbit; a gift from Kathryn
710 Anderson, Memorial Sloan Kettering Cancer Center, New York, NY; 1:500), anti-cone-arrestin
711 (rabbit; AB15282; Millipore; 1:500). Biotinylated SSTR3 and GPR161 were detected using
712 Alexa Fluor 647–labeled monovalent streptavidin (mSA647) (Ye et al., 2018). The following
713 reagents were used at the indicated concentrations: 200 nM SAG and 10 μM somatostatin 14.
714 Somatostatin 14 stocks were made in DMEM/F12 media, HEPES, no phenol red (11039-021,
715 GIBCO). SAG was dissolved in DMSO (276855, Sigma-Aldrich).

716 **Imaging and microscopy**

717 Cells were imaged either on a DeltaVision system (Applied Precision) equipped with a PlanApo
718 60x/1.40 objective lens (Olympus), CoolSNAP HQ2 camera (Photometrics), and solid-state
719 illumination module (InsightSSI), or on a confocal LSM 700 (Zeiss) microscope equipped with
720 40x Plan-Apochromat 1.3 DIC oil objective. Z stacks were acquired at 0.5 μm interval (LSM
721 700, Figs. 1, 2, 5, S1 and S2) or 0.2 μm interval (DeltaVision, Figs. 3 and 4).

722 For fixed imaging, 60,000 cells were seeded on acid-washed coverglass (12 mm #1.5; 12-545-81;
723 Thermo Fisher Scientific). Cells were grown for 24 h and then starved for 16-24 h in 0.2% FBS
724 media before experimental treatment. After treatment, cells were fixed with 4%
725 paraformaldehyde in PBS for 15 min at 37°C and extracted in -20°C methanol for 5 min. Cells
726 were then permeabilized in IF buffer (PBS supplemented with 0.1% Triton X-100, 5% normal
727 donkey serum (017-000-121; Jackson ImmunoResearch Laboratories), and 3% bovine serum
728 albumin (BP1605-100; Thermo Fisher Scientific)), incubated at room temperature for 1h with
729 primary antibodies diluted in IF buffer, washed three times in IF buffer, incubated with
730 secondary antibodies (Jackson ImmunoResearch Laboratories) diluted in IF buffer for 30 min,
731 and washed three times with IF buffer. DNA was stained with Hoechst 33258 (H1398; Molecular

732 Probes), cells were washed twice more with PBS, and coverglass mounted on slides using
733 fluoromount-G (17984-25; Electron Microscopy Sciences).

734 For live-cell imaging, 300,000 cells were seeded on acid-washed 25mm cover glass (Electron
735 Microscopy Sciences). After 24 h of growth, cells were serum starved for 16 h and transferred to
736 the DeltaVision stage for imaging at 37°C within an environmental chamber that encloses the
737 microscope and the stage. Cells were imaged in DMEM/F12 media, HEPES, no phenol red
738 (11039-021, GIBCO). To measure SSTR3 exit, cells expressing ^{AP}SSTR3 were first washed three
739 times with PBS and then pulse-labeled with 2µg/ml mSA647 for 5 min at 37°C. Cells were then
740 imaged after addition of sst (for SSTR3) or SAG (for GPR161) for 2 h with an acquisition every
741 10 min. Each acquisition consisted of a 3-plane Z-stack with each plane separated by 0.5 µm.
742 Transmittance was set to 5% and exposure time to 500 ms.

743 WT or *Bbs4*$^{-/-}$ mice (Mykytyn et al., 2004) eyes were enucleated at P21. Whole eyes were fixed in
744 4% paraformaldehyde/PBS overnight at 4°C and then washed three times with PBS. The eyes
745 were infiltrated in 30% sucrose/PBS at 4 °C overnight. Eyes were placed in OCT compound
746 embedding medium (4583; Tissue-Tek), frozen on dry ice, and stored at −80 °C. 14 µm sections
747 were cut on a cryostat (CM 1850; Leica). Sections were processed for immunofluorescence as
748 follows. Sections were blocked in blocking solution (50 mM Tris pH7.4, 100 mM NaCl, 0.1%
749 Triton-X 100, 3% normal donkey serum, and 0.1% BSA) for 1 h at room temperature, then
750 incubated with primary antibodies overnight at 4°C, followed by three washes in wash solution
751 (50 mM Tris pH7.4, 100 mM NaCl, and 0.1% TX100). After rinsing in wash solution, sections
752 were incubated with secondary antibodies for 1 h at room temperature. DNA was counterstained
753 using Hoechst 33258 dye, sections washed twice more with PBS, and mounted on slides using
754 Fluoromount-G. Sections were imaged on Confocal LSM 700 (Zeiss) microscope.

755

756 **Image analysis Bulk GPCR exit assays**

757 Files were imported from the Deltavision or LSM700 workstations into ImageJ/ Fiji (National
758 Institutes of Health) for analysis. For the quantification of ciliary ubiquitin signal in fixed cells,

759 maximum intensity projections were used. The ciliary ubiquitin intensity was measured using the
760 following equation:

761 $F_{Ub\text{-}cilia} = F_{Ub\text{-}cilia_measured} - F_{background}$

762 $F_{Ub\text{-}cilia_measured}$ is the total ciliary ubiquitin fluorescence detected, $F_{background}$ is the background
763 ubiquitin fluorescence measured in the adjacent area. For all measurements, the fluorescence
764 integrated density was used. No gamma adjustment was applied during figure preparation; all the
765 representative micrographs for respective panels are displayed within the same dynamic range.
766 For some representative micrographs, the most in-focus plane was used rather than the
767 maximum intensity projection (Fig.2, and Fig. 4, panel E and G).

768 To measure SSTR3 exit, for each time point, the integrated Alexa Fluor 647 fluorescence density
769 in the maximum intensity projection was measured using ImageJ. The cilia-adjacent fluorescence
770 was subtracted as the background, and a mathematical photobleaching correction was applied:

771 $F_{cilia} = (F_{mSA647_measured}/F_{mSA647_1}) + ((1 - e^{-\lambda}) * (n - 1))$, where λ is the photobleaching decay
772 constant, n is the number of images taken, $F_{mSA647_measured}$ is the integrated mSA647 fluorescence
773 measured for image n, F_{mSA657_1} is the measurement for the first time point, and F_{cilia} is the
774 reported fluorescence. In this equation, F_{cilia} is reported in relative fluorescence units (RFUs).
775 $^{AP}GPR161^{3NG}$ exit was followed similarly with the difference that NG fluorescence intensity was
776 measured.

777

778 **_Chlamydomonas_ culture, isolation of flagella and immunofluorescence**

779 *Chlamydomonas* WT- g1 (nit1, agg1, mt+) [gift from George B. Witman, University of
780 Massachusetts Medical School, Worcester, Massachusetts]and *Bbs4*- CC-4377 ptx5-1/bbs4-1::
781 NIT1 agg1 mt+ (Chlamydomonas Resource Center) strains were cultured asynchronously under
782 light in TAP media (Gorman and Levine, 1965) for 72 h. Flagellar fractions were prepared from
783 two liters of cultures of WT or *Bbs4* cells as described (Craige et al., 2013). Briefly, cells were
784 harvested by centrifugation for 5 min at 2,000 rpm (1,100 x *g*) at room temperature. Cells were

785 resuspended in 10 mM HEPES, pH 7.4 and centrifuged for 5 min at 2,000 rpm (1,100 x *g*). Next,
786 the cell pellet was gently resuspended in ice-cold HMDS (10 mM HEPES, pH 7.4, 5 mM
787 $MgSO_4$, 1 mM DTT, and 4% (w/v) sucrose). Deflagellattion was achieved by addition of 5 mM
788 dibucaine to each tube of cells and by pipetting up and down ~10 times using a 10-ml plastic
789 serological pipette. The suspension was spun for 5 min at 1,800 x *g* at 4°C. The supernatant
790 containing flagella was underlaid with 9 ml ice-cold HMDS-25% sucrose (10 mM HEPES, pH
791 7.4, 5 mM $MgSO_4$,1 mM DTT, and 25% (w/v) sucrose), followed by a centrifugation step for 10
792 min at 2,800 rpm (2,400 x *g*), 4°C. The supernatant above the sucrose interface was collected
793 using a 25-ml serological pipette and flagella were pelleted by centrifugation for 20 min at 30,000
794 x *g* (16,000 rpm), 4°C. The flagellar pellet was resuspended in 100 µl HMDS buffer. Protein
795 concentrations were measured by Bradford and 25 ug were resolved by SDS-PAGE for
796 immunoblotting.

797 *Chlamydomonas* immunofluorescence was performed as follows. Cells were fixed with 4 %
798 paraformaldehyde in MT buffer* (30 mM HEPES, pH7, 5 mM EGTA, 5 mM MgSO4, and
799 25mM KCl) for 20 minutes in suspension. The cells were centrifuged at 1000 rpm for 5 minutes,
800 resuspended in 100 µl of fixative and transferred onto slides coated with 1 mg/ml poly-L-lysine.
801 After 5 minutes, the unadhered cells were washed off by rinsing with PBS. Cells were
802 permeabilized in 0.5% Triton-X 100 for 20 minutes followed by blocking for 1 h in blocking
803 buffer (3% fish skin gelatin, 1% BSA, 0.1% Tween20 in PBS) at room temperature. Cells were
804 incubated at 4°C overnight with primary antibodies diluted in blocking buffer, washed five times
805 in PBS and incubated with secondary antibodies for 2 h at room temperature. After five washes
806 in PBS, coverglasses were mounting on slides using Fluoromount-G. Cells were imaged on the
807 LSM700 confocal microscope.